blood®
Regular Article

GENE THERAPY

An erythroid-specific lentiviral vector improves anemia and iron metabolism in a new model of XLSA

Carlo Castruccio Castracani,[1] Laura Breda,[1] Tyler E. Papp,[2] Amaliris Guerra,[1] Enrico Radaelli,[3] Charles-Antoine Assenmacher,[3] Giovanni Finesso,[3] Barbara L. Mui,[4] Ying K. Tam,[4] Simona Fontana,[5] Chiara Riganti,[5] Veronica Fiorito,[6] Sara Petrillo,[6] Emanuela Tolosano,[6] Hamideh Parhiz,[2] and Stefano Rivella[1,7-10]

[1]Department of Pediatrics, Hematology, The Children's Hospital of Philadelphia, Philadelphia, PA; [2]Department of Systems Pharmacology and Translational Therapeutics, Perelman School of Medicine, University of Pennsylvania, Philadelphia, PA; [3]Comparative Pathology Core, Department of Pathobiology, University of Pennsylvania School of Veterinary Medicine, Philadelphia, PA; [4]Acuitas Therapeutics, Vancouver, British Columbia, Canada; [5]Department of Oncology and [6]Department of Biotechnology and Health Sciences and Molecular Biotechnology Center "Guido Tarone," University of Torino, Torino, Italy; [7]University of Pennsylvania, Perelman School of Medicine, Philadelphia, PA; [8]Raymond G. Perelman Center for Cellular and Molecular Therapeutics–The Children's Hospital of Philadelphia, Philadelphia, PA; [9]Penn Center for Musculoskeletal Disorders, The Children's Hospital of Philadelphia, Philadelphia, PA; and [10]Penn Institute for RNA Innovation, University of Pennsylvania, Philadelphia, PA

KEY POINTS

- We characterized erythropoiesis and iron metabolism in a new model of XLSA, showing ring sideroblasts and mitochondrial iron accumulation.
- We used a novel and lentiviral vector expressing the human *ALAS2* gene to rescue these animals from lethal anemia.

X-linked sideroblastic anemia (XLSA) is a congenital anemia caused by mutations in *ALAS2*, a gene responsible for heme synthesis. Treatments are limited to pyridoxine supplements and blood transfusions, offering no definitive cure except for allogeneic hematopoietic stem cell transplantation, only accessible to a subset of patients. The absence of a suitable animal model has hindered the development of gene therapy research for this disease. We engineered a conditional *Alas2*-knockout (KO) mouse model using tamoxifen administration or treatment with lipid nanoparticles carrying Cre-mRNA and conjugated to an anti-CD117 antibody. *Alas2*-KO^{BM} animals displayed a severe anemic phenotype characterized by ineffective erythropoiesis (IE), leading to low numbers of red blood cells, hemoglobin, and hematocrit. In particular, erythropoiesis in these animals showed expansion of polychromatic erythroid cells, characterized by reduced oxidative phosphorylation, mitochondria's function, and activity of key tricarboxylic acid cycle enzymes. In contrast, glycolysis was increased in the unsuccessful attempt to extend cell survival despite mitochondrial dysfunction. The IE was associated with marked splenomegaly and low hepcidin levels, leading to iron accumulation in the liver, spleen, and bone marrow and the formation of ring sideroblasts. To investigate the potential of a gene therapy approach for XLSA, we developed a lentiviral vector (X-ALAS2-LV) to direct *ALAS2* expression in erythroid cells. Infusion of bone marrow (BM) cells with 0.6 to 1.4 copies of the X-ALAS2-LV in *Alas2*-KO^{BM} mice improved complete blood cell levels, tissue iron accumulation, and survival rates. These findings suggest our vector could be curative in patients with XLSA.

Introduction

Sideroblastic anemia is a group of congenital and acquired disorders that presents the characteristic bone marrow (BM) sideroblasts, a sign of excessive mitochondrial deposition of iron.[1,2] The congenital forms (congenital sideroblastic anemia) are rare and caused by mutations in the genes involved in heme biosynthesis, Fe-S cluster, and mitochondrial protein synthesis.[2,3] X-linked sideroblastic anemia (XLSA) is the most common form of congenital sideroblastic anemia caused by germline mutations in the erythroid-specific 5-aminolevulinate synthase (*ALAS2*) gene, encoding for the enzyme ALAS2.[1,3] ALAS2 plays a crucial role in heme biosynthesis, specifically in erythroid cells.[4] Being the first and rate-limiting enzyme in the heme biosynthetic pathway, ALAS2 catalyzes the condensation of glycine and succinyl-CoA to form 5-aminolevulinic acid.[5] *ALAS2* expression is not inhibited by high heme levels and is positively regulated by hypoxia.[6] Typically, patients affected by the XLSA are hemizygous males who exhibit the disease before the age of 40 years, with hypochromic microcytic anemia and systemic iron overload.[1-3,7] Heterozygous female carriers might develop the disease because of a non–well-defined mechanism, possibly related to skewed X-chromosome inactivation.[8-14] Most mutations result in partial loss of function.[2,15-17] Vitamin B6 is the first-line treatment for XLSA, but almost 50% of the cases are unresponsive.[3,18,19] Oral 5-aminolevulinic acid supplementation has failed as a second-line treatment in vitamin B6-refractory XLSA.[20]

Gene therapy strategies for hemoglobinopathies, such as β-thalassemia and sickle cell disease, aim to introduce, by lentiviral vectors (LVs), functional copies of the globin genes into patient hematopoietic stem cells (HSCs) to restore normal hemoglobin (Hb) production.[21] One established approach involves using erythroid-specific vectors, tailoring the expression of erythroid genes in red blood cell (RBC) precursors. LVs have shown significant promise in gene therapy due to efficiently transducing dividing and nondividing cells, such as HSCs.[22] LVs can accommodate larger gene inserts (such as the *ALAS2* gene and erythroid regulatory sequences), essential for heme synthesis and typically active in late-stage erythropoiesis.[22,23] Furthermore, recent LVs have been extensively researched and modified to enhance safety and specificity.[24,25] Therefore, ex vivo HSC gene therapy using an LV represents a potential therapeutic option, improving patients' conditions by supplying a functional copy of the *ALAS2* cDNA. Considering the rarity of the disease, the lack of therapeutic options, and the elevated number of mutations causing the disease, it is essential to establish a severe phenotype and study whether an erythroid-specific *ALAS2*-LV would be effective in reversing the most severe form of the disease.

In this study, we established a severe murine model of XLSA through 2 distinct methods. The *Alas2*-knockout (KO)^{BM} animals exhibited severe anemia, mitochondrial dysfunction, altered iron metabolism, ring sideroblasts, and mitochondrial iron accumulation. Moreover, we successfully developed an erythroid-driven LV capable of effectively improving the disease phenotype. These results mark a significant step toward the characterization of this disease and potentially new therapeutic interventions for patients afflicted with this rare disorder.

Materials and methods

Mouse lines and breeding conditions

R26-CreER^{T2}(RRID:IMSR_JAX:008463),B6.SJL-Ptprc^{a}Pepc^{b}/BoyJ(RRID:IMSR_JAX:002014) mice were purchased from The Jackson Laboratory (Bar Harbor, ME) or as described (supplemental Figure 1A-B [available on the *Blood* website]).

Vector production and characterization of X-ALAS2-LV

To create viral stocks, the *ALAS2* gene-transfer plasmid was cotransfected with the envelope plasmid (VSV-G), the packaging plasmid (pMDLg/pRRE), and the pRSVREV vector into HEK293T cells, according to Breda et al.[26] The multiplicity of infection (MOI) was calculated using the following formula: number of cells (5×10^4) × dilution factor (1 mL/μL viral preparation) × vector copy number (VCN) (measured using a droplet digital polymerase chain reaction probe specific for the Psi sequence found in lentiviral vectors). To determine the optimal MOI of X-ALAS2-LV for ex vivo transduction of HSC, serial dilutions of concentrated viral preparations were used to transduce NIH-3T3 and HUDEP-2 cells. VCN was evaluated by droplet digital polymerase chain reaction (Figure 1B). The titer was 1.10E+09 infection particle/mL in NIH-3T3 cells and 3.7E+10 infection particle/mL in HUDEP-2 cells.

Results

Generation of a conditional Alas2-KO transgenic line

A complete knockout of the *Alas2* gene is expected to be lethal.[27,28] Therefore, we pursued an inducible conditional KO model as a feasible alternative to reproduce a complete *Alas2*-KO model. We generated transgenic *Alas2*$^{fl/fl}$ mice designed with LoxP sites flanking a critical segment of the *Alas2* mouse gene upstream and downstream of exon 5, as deletion of this exon is expected to result in the formation of a stop codon at the beginning of exon 6 and the loss of functional ALAS2 (supplemental Figure 1A-B). The mice carrying the LoxP sites were crossed with the well-characterized 26-CreER^{T2} Cre strain,[29] where the Cre-ER^{T2} (Cre recombinase–estrogen receptor T2) cassette is introduced into the ROSA locus. Tamoxifen (TAM) administration induces the translocation of Cre recombinase from the cytoplasm to the nucleus from the ER^{T2} moiety, allowing the recombination of genomic LoxP sites. The F_1 generation consisted of R26-CreER$^{T2+/+}$-*Alas2*$^{fl/+}$ mice, which were further crossed to obtain the R26-CreER$^{T2+/+}$-*Alas2*$^{fl/Y}$ genotype or F_2 generation (supplemental Figure 1A).

Administration of TAM determined the development of anemia (Figure 2A) and ineffective erythropoiesis (IE) (Figure 2B). IE in the BM and the spleen of the R26-CreER$^{T2+/+}$-*Alas2*$^{fl/Y}$ mice was characterized by the expansion of the proerythroblast/basophilic erythroblast population (P1/P2) and the polychromatic erythroid population (P3). In contrast, the orthochromatic/reticulocyte (P4) and RBC populations (P5) were reduced. KO mice were sacrificed or succumbed due to severe anemia. To rigorously establish that the observed phenotype was not solely attributed to TAM administration, we administered TAM in R26-Cre$^{ERT2+/+}$-*Alas2*$^{+/Y}$ mice, which lack the flox sites. On treatment, we observed only a temporary reduction in RBCs (P5) with concurrent expansion of the orthochromatic/reticulocyte population (P4), an effect that was reversed after 21 days. These alterations were consistent with the known effects of TAM use and led to mild but transient anemia, as evidenced by subsequent recovery (Figure 2A). This experiment reinforces our conclusion, demonstrating that the persistence of disease phenotype was independent of TAM administration. Having observed that complete deletion of *Alas2* in mice showed erythroid-specific pathophysiology, we focused on deleting the *Alas2* gene only in the hematopoietic compartment.

Alas2-KO in the BM leads to IE and severe anemia

The first approach was based on the engraftment of R26-CreER^{T2}-*Alas2*$^{fl/Y}$ Lin$^-$ HSCs into lethally irradiated wild-type (WT) mice, namely B6. SJL-Ptprc^{a}Pepc^{b}/BoyJ mice (supplemental Figure 1C). Eight weeks after transplantation, the mice were treated with the same dose of TAM used for the previous experiments. As an alternative approach, we used lipid nanoparticles (LNPs) embedded with a Cre mRNA and decorated with an antibody targeting the CD117 receptor (LNP^{CD117}Cre) to induce the deletion of the *Alas2* gene ex vivo (supplemental Figure 1C) in HSC.[30] Lin$^-$ HSCs *Alas2*$^{fl/Y}$ cells showed high levels of *Alas2* deletion after 24 hours and a complete absence of *Alas2* after 72-hour incubation with LNP^{CD117}Cre (Figure 2C). Using this approach, we then injected lethally irradiated WT mice with Lin$^-$ cells *Alas2*$^{fl/Y}$ freshly treated ex vivo by LNP^{CD117}Cre. To assess the extent of *Alas2*

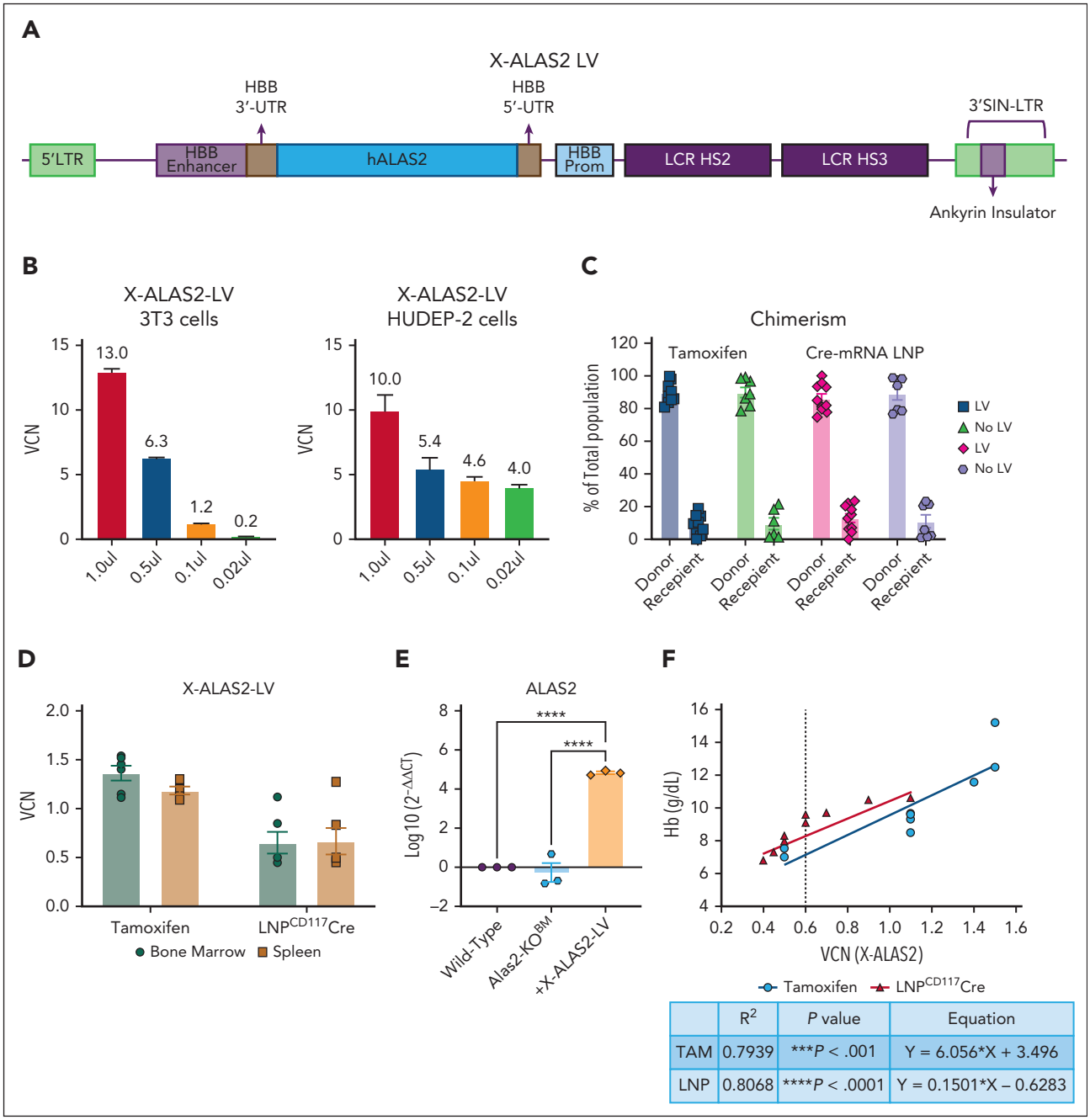

	R^2	*P* value	Equation
TAM	0.7939	***$P < .001$	Y = 6.056*X + 3.496
LNP	0.8068	****$P < .0001$	Y = 0.1501*X – 0.6283

Figure 1. Characterization of the new lentiviral vector X-ALAS2-LV. (A) Schematic diagram of X-ALAS2 lentiviral vector. (B) VCN analysis of X-ALAS2-LV in NIH-3T3 and HUDEP-2 cells. N = 3 for each LV concentration; the results are shown as median ± SD. (C) Chimerism analysis after BM transplantation (N = 9 for each experimental group). Data are shown as mean ± standard error of the mean (SEM). (D) X-ALAS2-LV VCN analysis 25 weeks after transplantation in the BM and spleen (SPL) samples from TAM and LNP^{CD117}Cre models (N = 6 in all experimental groups). Data are shown as mean ± SEM. (E) Quantification of human *Alas2* gene expression (quantitative reverse transcription polymerase chain reaction [qRT-PCR]) in Lin$^-$ cells from *Alas2*$^{fl/Y}$ BM. *P* values are determined by the Tukey multiple-comparison test after the 1-way ANOVA. ****$P < .0001$. (F) Correlation of VCN (X-ALAS2-LV) and Hb (g/dL) values in the TAM and LNP^{CD117}Cre models in X-ALAS2 treated mice. *P* values, R squared, and curve equations are obtained by simple linear regression analysis. Treatment with X-ALAS2-LV extended the survival of animals with VCN <0.6, although these mice eventually showed progressive anemia that required their sacrifice. In animals with VCN >0.6 instead, treatment with X-ALAS2-LV improved the disease phenotype.

gene deletion following either TAM administration or infusion of HSC treated with LNP^{CD117}Cre, we quantified the abundance of the *Alas2* allele in mouse BM by digital droplet PCR assay using a probe/primer set specifically designed to amplify the region between exon 5 and exon 6 of *Alas2* (supplemental Table 3). Compared with TAM, the LNP-mediated delivery of Cre recombinase was more effective and faster in deleting the target gene (Figure 2D).

Both experimental groups, infused with LNP^{CD117}Cre treated *Alas2*$^{fl/Y}$ HSC or R26-CreER^{T2}-*Alas2*$^{fl/Y}$ HSC followed by TAM treatment, showed that the deletion of the *Alas2* gene led to the development of severe anemia. In animals transplanted with LNP^{CD117}Cre treated *Alas2*$^{fl/Y}$ HSC, the recipient mice received HSC already deleted of the *Alas2* gene. In animals engrafted with R26-CreER^{T2}-*Alas2*$^{fl/Y}$ HSC, the deletion was induced with TAM 8 weeks after engraftment. Nevertheless, the end points

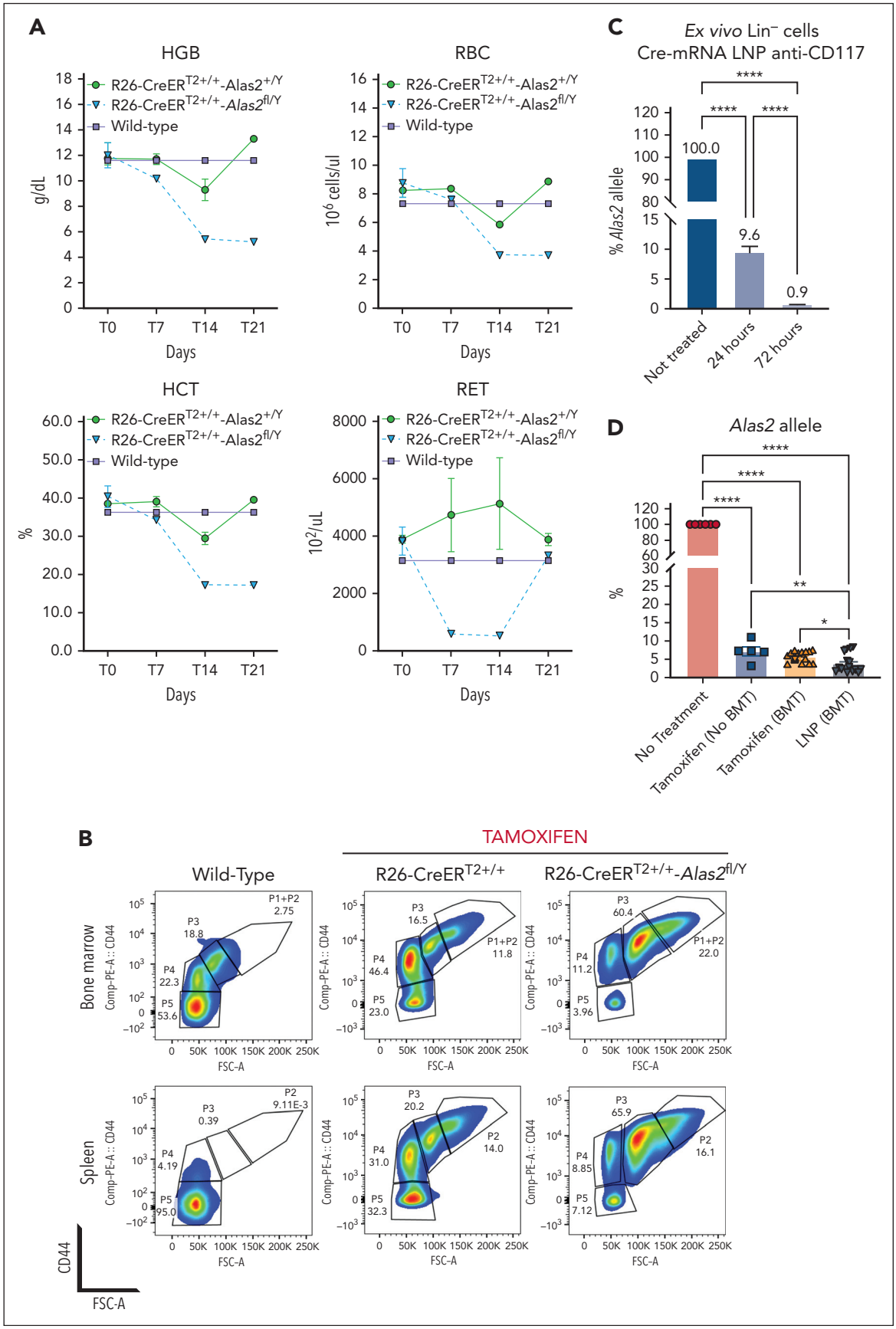
A
HGB
RBC
HCT
RET
R26-CreER$^{T2+/+}$-Alas2$^{+/Y}$
R26-CreER$^{T2+/+}$-*Alas2*$^{fl/Y}$
Wild-type
g/dL
10^6 cells/ul
%
10^2/uL
T0
T7
T14
T21
Days
C
Ex vivo Lin⁻ cells
Cre-mRNA LNP anti-CD117
% *Alas2* allele
100.0
9.6
0.9
Not treated
24 hours
72 hours
****
D
Alas2 allele
%
No Treatment
Tamoxifen (No BMT)
Tamoxifen (BMT)
LNP (BMT)
**
*
B
TAMOXIFEN
Wild-Type
R26-CreER$^{T2+/+}$
R26-CreER$^{T2+/+}$-*Alas2*$^{fl/Y}$
Bone marrow
Spleen
Comp-PE-A :: CD44
FSC-A
P1+P2 2.75
P3 18.8
P4 22.3
P5 53.6
P3 16.5
P1+P2 11.8
P4 46.4
P5 23.0
P3 60.4
P1+P2 22.0
P4 11.2
P5 3.96
P2 9.11E-3
P3 0.39
P4 4.19
P5 95.0
P3 20.2
P2 14.0
P4 31.0
P5 32.3
P3 65.9
P2 16.1
P4 8.85
P5 7.12
CD44
FSC-A

Figure 2.

were comparable (severe lethal anemia; Figure 3A). Importantly, the animals transplanted with R26-CreER^{T2}-*Alas2*$^{fl/Y}$ HSC and treated with TAM recapitulated the phenotype observed in animals with a total body deletion of *Alas2* (Figure 2A).

KO animals exhibited pronounced anemia, marked by diminished Hb levels and RBC count. Additionally, they exhibited decreased hematocrit (HCT) and mean corpuscular volume levels (Figure 3A; Table 1). Eventually, no animal survived without expression of *Alas2*. However, we observed a difference in the onset of the anemia between the 2 cohorts, given the faster development of the phenotype and earlier death observed in the LNP^{CD117}Cre-induced model (deletion induced in HSC in vitro, before engraftment) vs the TAM model (deletion induced ~8 weeks after BM transplant [BMT]) (Figure 3B).

We also characterized erythroid maturation in BM and spleen cells using specific Ter119, CD71, and CD44 markers.[31] The *Alas2*-KO^{BM} phenotype was associated with a substantial reduction in mature erythroid cells, with an elevated number of polychromatic erythroblasts (P3) in the BM and spleen (Figure 3C; supplemental Figure 2A). Blood smears from these mice revealed a heterogeneous population of RBCs, including hypochromic RBCs (Figure 3D) and increased reticulocyte count (Figure 3A). In physiological erythropoiesis, the expression of *Alas2*, *Alas1*, and *Tfrc* in the erythroid populations is correlated with the differentiation of the erythroid populations. The expression of *Alas2* is directly associated with the progressive differentiation of the erythroid populations, with the peak of expression in the orthochromatic erythroblasts (P4). On the contrary, the expression of *Alas1*, the ubiquitous isoform of *Alas*, was almost suppressed across the differentiation from proerythroblasts (P1) to basophilic erythroblasts (P2) (supplemental Figure 2B). The *Tfrc* levels also correlate with the progression of differentiation of the erythroid population under partial regulation of erythropoietin, ensuring the survival and proliferation of erythroblasts, leading to the restoration of oxygenation through RBC production (supplemental Figure 2B).[32] These findings highlight the significance of *Alas2*, in contrast to *Alas1*, during this critical stage of erythroid development. These observations suggest that erythroid populations at this stage initiate iron accumulation, underscoring the importance of *Alas2* in this iron homeostasis regulation. Furthermore, these results provide compelling support for the *Alas2*-KO^{BM} phenotype, wherein the absence of *Alas2* disrupts the differentiation of polychromatic erythroblasts (P3) into orthochromatic erythroblasts (P4) and, consequently, impedes the production of functional RBCs.

Alas2-KO^{BM} mice showed severe splenomegaly associated with abnormal color and consistency. The paler color (pink vs red in WT mice) in the spleen of *Alas2*-KO^{BM} mice likely indicated decreased heme synthesis and iron accumulation (Figure 4A). The most consistent alterations in the spleen were extramedullary hematopoiesis and lymphoid hyperplasia (Figure 4B). Histologic analysis showed extramedullary hematopoiesis in the liver and brownish pigment accumulation, consistent with hemosiderin formation. The most consistent alterations in the BM were erythroid hyperplasia and a similar brown pigmentation accumulation (Figure 4C; supplemental Figure 3A-B). In both organs, hematopoiesis is strongly skewed toward the erythroid lineage. In all organs of most mice, blood vessels frequently contained smaller erythrocytes and erythrocytes with a basophilic cytoplasm. This change was most prominent in the BM (supplemental Figure 3A). In the liver, clusters of varying-sized cells are distributed randomly throughout the hepatic parenchyma, containing abundant cytoplasmic iron accumulation. These cells likely consist of Kupffer cells and other macrophages (supplemental Figure 3C). Abnormal iron accumulation was observed in several tissues of mice lacking the *Alas2* gene (Figures 4B-C and 5A). Notably, the iron staining of bone marrow tissues and smears confirmed the presence of ring sideroblasts (Figure 5B), and the electron microscopy analysis revealed iron deposits in the mitochondria (Figure 5C). To confirm the dysregulation of iron homeostasis, we evaluated erythroferrone (ERFE) and hepcidin (HAMP) serum levels. Diseases characterized by IE are generally associated with high levels of erythropoietin (EPO) and ERFE and low levels of HAMP, leading to increased iron absorption and organ iron overload.[33] *Alas2*-KO^{BM} animals showed increased ERFE and decreased HAMP levels, consistent with increased EPO, serum iron levels, and organ iron overload. We also observed increased ferritin levels and transferrin saturation due to IE, increased gastrointestinal iron absorption, and subsequent systemic iron overload due to compensation for defective heme synthesis, leading to excess iron in both storage and circulating forms (Figure 6A).

Alas2 KO causes a shutdown of the mitochondria in the polychromatic erythroid population

To further characterize the impact of *Alas2*-KO on the erythroid population, we performed metabolic assays focusing on isolated polychromatic erythroid cells in R26-CreER$^{T2+/+}$-*Alas2*$^{fl/Y}$ mice that underwent TAM treatment (P3). We focused on P3 as this was the most abnormally elevated erythroid population (Figure 2B). At the onset of the anemia, the P3 population in the BM was sorted. Cells were then analyzed by ultraperformance liquid chromatography. Moreover, we measured the activity of ALAS2, the key enzymes in the tricarboxylic acid cycle, the electron transport chain (ETC) complexes, and the level of mitochondrial adenosine triphosphate (mtATP). As expected, *Alas2*-KO^{BM} P3 cells presented a significant and robust reduction of ALAS2 activity compared with the WT P3 population. Notably, the diminished ALAS2 activity correlated with the

Figure 2. Evaluation of the use of Tamoxifen and LNP^{CD117}Cre in a conditional *Alas2*-KO model. (A) Values of Hb, RBC, HCT, and reticulocytes (RETs) in R26CreER^{T2} and R26CreER^{T2}-*Alas2*$^{fl/Y}$ animals after administration of TAM. N = 4 for each group. Data are shown as mean ± standard error of the mean (SEM). (B) Representative flow cytometry analysis of the erythroid populations in the BM and spleen in R26CreER^{T2} and R26CreER^{T2}-*Alas2*$^{fl/Y}$ animals treated with TAM. Data are shown as FSC-A/CD44 subgated on the Ter119^{+} population. P1+P2/P2 = proerythroblasts/basophilic erythroblasts; P3 = polychromatic erythroblasts; P4 = orthochromatic erythroblasts/reticulocytes; P5 = erythrocytes. (C) Quantification of *Alas2* allelic deletion (droplet digital polymerase chain reaction [ddPCR] analysis) of gDNA isolated from Lin^{-} cells from *Alas2*$^{fl/Y}$ BM after exposure to LNP^{CD117}Cre. Data are shown as mean ± SEM (N = 3 independent replicates). *P* values are determined by the Tukey multiple-comparison test after the 1-way analysis of variance (ANOVA). **** $P < .0001$. (D) Quantification of *Alas2* allelic deletion (ddPCR analysis) of gDNA isolated from Lin^{-} cells from *Alas2*$^{fl/Y}$ BM, after tamoxifen treatment (with or without BMT) or exposure to LNP^{CD117}Cre. Data are shown as mean ± SEM (N = 3 independent replicates). *P* values are determined by the Tukey multiple-comparison test after the 1-way ANOVA. *$P < .05$, **$P < .001$, **** $P < .0001$.

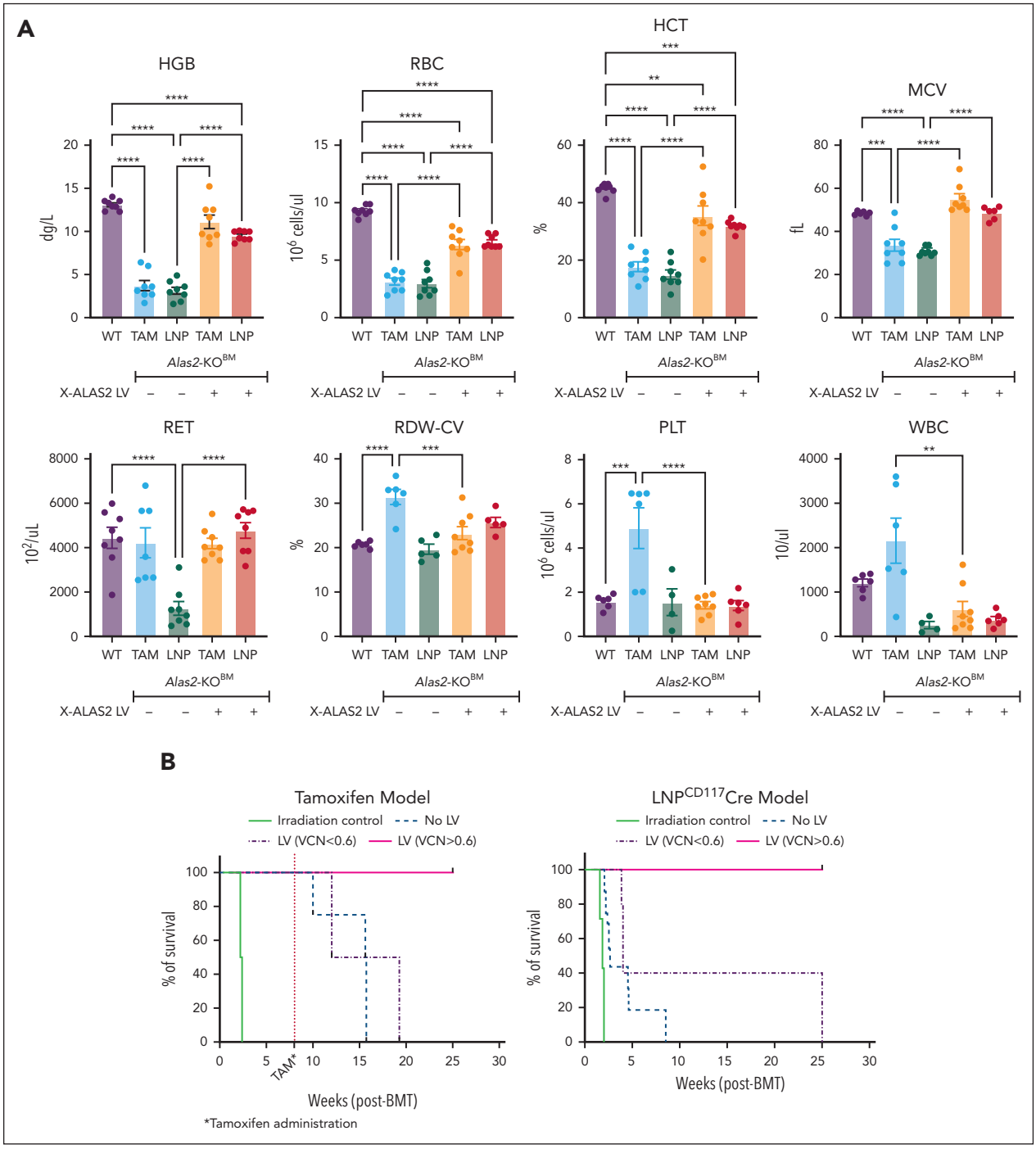

Figure 3. Characterization of anemia, survival and ineffective erythropoiesis of *Alas2*-KO^{BM} mice in presence of absence of X-ALAS2-LV. (A) Complete blood cell (CBC) panel at the end point in each experimental group. Each model includes animals treated (+) and not treated (–) with X-ALAS2-LV (N = 8 in all experimental groups). Data are shown as mean ± standard error of the mean (SEM). *P* values are determined by the Tukey multiple-comparison test after the 1-way analysis of variance (ANOVA). $^{**}P < .01$, $^{***}P < .001$, $^{****}P < .0001$. Although there is not a significant difference in the *Alas2*-KO^{BM} animals treated with tamoxifen or LNP^{CD117}Cre, the LNP-treated animals did show a reduced absolute reticulocyte count (ARC) compared with the tamoxifen model. Compared with tamoxifen, the LNP technology is more efficient in deleting *Alas2* (as shown in Figure 2D), and the cells engrafted already lack the *Alas2* gene. In the tamoxifen approach, the process to delete the target gene is slower (as this requires repeated administration of tamoxifen), and more undeleted cells may be present, which still possess the ability to regenerate and mature into reticulocytes. However, these cells are insufficient to support normal erythropoiesis and rescue the animals. (B) Kaplan-Meier analysis of experimental cohorts in TAM and the LNP^{CD117}Cre models. Each model includes animals treated (LV) and not treated (No LV) with X-ALAS2-LV (N = 9 in all experimental groups). Curve comparison in the TAM model: $P < .001$, $\chi^2 = 17.50$ in the Mantel-Cox test. Curve comparison in the LNP^{CD117}Cre model: $P < .01$, $\chi^2 = 14.18$ in the Mantel-Cox test. (C) Representative flow cytometry analysis of the BM and spleen erythroid cells defined by FSC-A/CD-44 within the Ter119$^+$ pregated population in TAM and LNP^{CD117}Cre models. An example of an X-ALAS2 lentiviral vector and nontreated samples (*Alas2*-KO^{BM}) are shown for each model. P1+P2/P2 = proerythroblasts/basophilic erythroblasts; P3 = polychromatic erythroblasts; P4 = orthochromatic erythroblasts/reticulocytes; P5 = erythrocytes. (D) Representative blood smears of each experimental group, in animals treated (+X-ALAS2-LV) or not treated (No Vector) with X-ALAS2-LV, from TAM and LNP^{CD117}Cre cohorts.

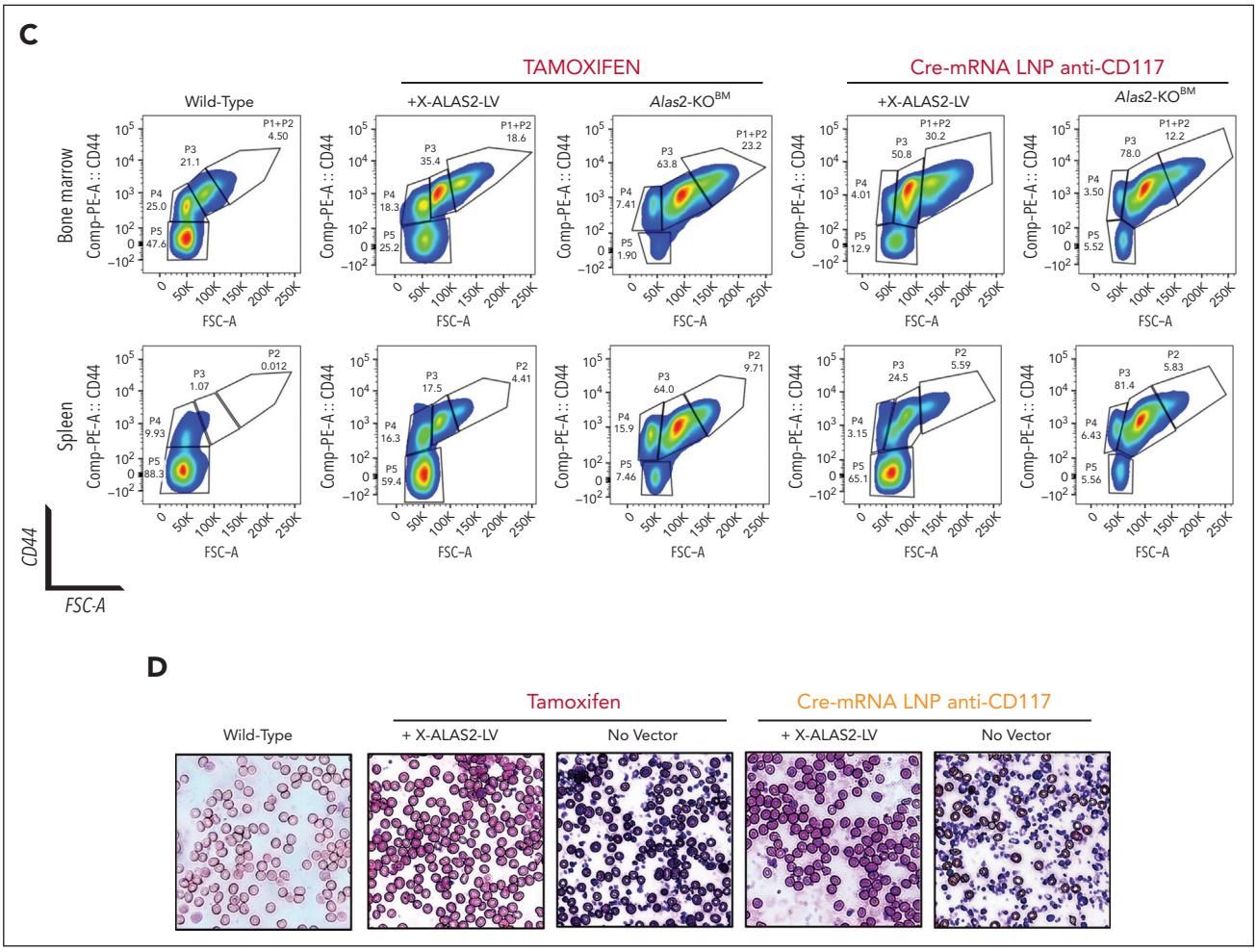

Figure 3 (continued)

shutdown of oxidative metabolism, as indicated by the substantially lowered activity of pivotal tricarboxylic acid cycle enzymes, such as citrate synthase, α-ketoglutarate dehydrogenase, succinate dehydrogenase, and malate dehydrogenase, as well as by a considerable reduction in the activity of mitochondrial ETC complexes. In line with this, mtATP levels were also significantly decreased in the *Alas2*-KO^{BM} P3 population (Figure 6B). The data are further supported by the electron microscopy analysis of the mitochondrial cristae (supplemental Figure S4), showing an increased area and perimeter with a typical perturbed unfolded shape in the *Alas2*-KO^{BM} P3 population. In this nonphysiological scenario, the ETC supercomplexes and dimers of adenosine triphosphate synthase disassemble, decreasing mitochondrial respiratory performance.[34] The analysis of the glycolytic profile in *Alas2*-KO^{BM} P3 cells showed increased activity of glycolytic enzymes compared

Table 1. Mean values of Hb, RBC, HTC, and RET at the end point in each experimental group

	WT		Tamoxifen				LNP^{CD117}Cre			
	C57BL/6J		X-ALAS2-LV		*Alas2*-KO^{BM}		X-ALAS2-LV		*Alas2*-KO^{BM}	
Variable	Mean	SEM	Mean	SEM	Mean	SEM	Mean	SEM	Mean	SEM
Hb, g/dL	13.1	0.21	11.1	0.79	3.7	0.58	9.5	0.20	3.1	0.39
RBC, 10^6 cells/μL	9.3	0.16	6.4	0.46	3.2	0.29	6.6	0.19	3.0	0.37
HCT, %	44.8	0.60	35.4	3.41	17.7	1.66	31.9	0.63	14.9	1.61
RET, 10^2 cells/μL	4442.5	464.5	4168.0	252.6	4222.6	670.3	4771.0	355.7	1262.8	308.0

Each model includes animals treated (X-ALAS2-LV) and not treated (*Alas2*-KO^{BM}) with X-ALAS2-LV (N = 8 in all experimental groups).
RET, reticulocyte; SEM, standard error of the mean.

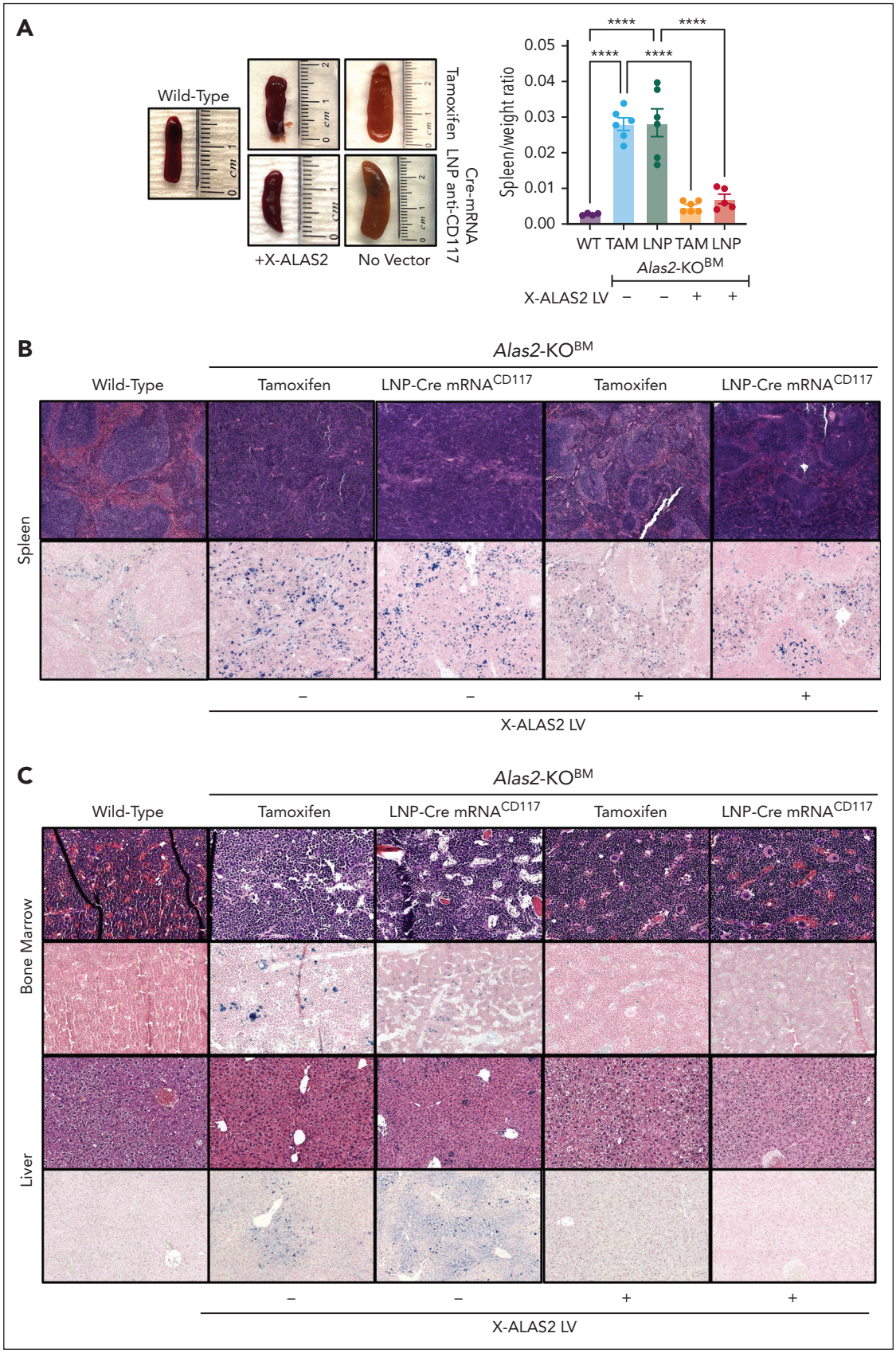

Figure 4. Pathological evaluation of spleen, liver and bone marrow of *Alas2*-KO^{BM} animals in presence or absence of X-ALAS2-LV. (A) Quantification of the spleen/body weight ratio in animals treated (+) or not treated (–) with X-ALAS2-LV (N = 9 in all experimental groups) from TAM (TAM) and LNP^{CD117}Cre (LNP) models at the end point of each experimental group. Data are shown as mean ± standard error of the mean (SEM). *P* values are determined by the Tukey multiple-comparison test after 1-way analysis of variance (ANOVA). ****$P < .0001$. Representative pictures of spleens were collected at the end point of each experimental group. (B) Representative images of hematoxylin and eosin (H&E)

with the control, supported by transcriptional reprogramming (Figure 6C-D).

Interestingly, the expression of some components of the respiratory chain complexes yielded opposite results compared with the enzymatic activity (Figure 6B-D). This suggests a compensatory response to the reduced activity, possibly indicating an increase in gene expression related to the oxydative phosphorylation (OXPHOS) malfunction. These results further highlighted the altered erythropoiesis observed in the BM, underscoring the crucial role of ALAS2 in the differentiation and maturation of polychromatic erythroid cells to orthochromatic cells. The inability of *Alas2*-KO^{BM} cells to robustly differentiate is likely to promote cell death, as suggested by the relative increase of proapoptotic genes in the P3 population (Figure 7A). A further assessment showed an increased tendency toward inflammation in the P3 population (Figure 7B). These results shed light on how the reduction of ALAS2 activity in hypomorphic patients disrupts the erythropoietic development, leading to diminished production of RBCs.[28]

Generation of an erythroid-specific lentiviral vector to express the human ALAS2 cDNA

To develop a definitive curative therapeutic option for severe forms of XLSA, we generated a novel gene therapy lentiviral vector expressing the human *ALAS2*, specifically the *Homo sapiens* 5′-aminolevulinate synthase 2, transcript variant 1 (NM_000032.5). To allow exclusive erythroid expression, the *ALAS2* gene was cloned under the control of an erythroid-specific promoter (hemoglobin subunit beta [HBB] promoter, 200 bp) into a lentiviral backbone previously described.[26] To ensure controlled expression of *ALAS2* cDNA in the erythroid compartment, the vector included additional sequences used to express the β-globin gene, such as the 3′ HBB enhancer (876 bp) and the hypersensitive sites 2 (HS2) (1435 bp) and 3 (HS3) (1202 bp) of the locus control region.[35,36] These sequences have been extensively studied and proven effective in achieving elevated levels of erythroid-specific expression both in vitro and in vivo.[36] Moreover, we included the ankyrin insulator (190 bp) embedded in the vector's 3′ self-inactivating long terminal repeat, as previous studies suggested that including this element reduces integration position effects on expression and genome toxicity, resulting in a safer vector overall (Figure 1A; supplemental Table 2).[35,37-43] To characterize and determine the optimal concentration of X-ALAS2-LV for in vivo application, we measured vector potency by transducing NIH-3T3 and HUDEP-2 cells (Figure 1B).

X-ALAS2 lentivirus improves the Alas2-KO^{BM} phenotype

We tested the X-ALAS2-LV vector's ability to reverse the anemia in the *Alas2*-KO^{BM} murine models. For the TAM model, we isolated R26-CreER^{T2}-*Alas2*$^{fl/Y}$ Lin$^-$ HSCs. Some of the cells were exposed to 100 to 150 MOI of X-ALAS2-LV. Transduced and nontransduced cells were then separately infused into lethally irradiated B6. SJL-Ptprc^{a}Pepc^b/BoyJ mice (supplemental Figure 1C). As controls, we transplanted untreated R26-CreER^{T2} Lin$^-$ HSCs into recipient animals. For the LNP model, *Alas2*$^{fl/Y}$ Lin$^-$ HSCs were isolated and incubated with LNP^{CD117}Cre for 2 hours before transduction with X-ALAS2-LV (100-150 MOI) (supplemental Figure 1C). As controls, we transplanted untreated *Alas2*$^{fl/Y}$ Lin$^-$ HSCs. Donor chimerism was evaluated 8 weeks after transplantation. In the TAM model, donor chimerism reached 90% (±2.0%) and 89.8% (±3.1%) in the treated and untreated animals, respectively, whereas in the LNP^{CD117}Cre model, donor chimerism levels were 86.2% (±2.7%) and 89.0% (±3.8%) in the treated and untreated animals, respectively (Figure 1C). The VCN in BM and spleen in both the TAM and LNP^{CD117}Cre experimental settings was stable up to 25 weeks after transplantation (Figure 1D). In the TAM settings, the VCN in the BM of X-ALAS2-LV treated animals ranged between 0.5 and 1.5, whereas in the LNP^{CD117}Cre counterpart, the VCN ranged between 0.5 and 1.1. Animals with VCNs lower than 0.6 showed extended lifespan compared with untreated animals, yet the expression of *ALAS2* produced by the transgene was insufficient to reverse the anemia; hence, these animals were euthanized for analyses when Hb levels reached ~7.0 g/dL (Figure 3B). In these animals, we observed an expansion of the polychromatic erythroid (P3) population and mild splenomegaly (data not shown), with a phenotype intermediate between the complete KO and animals rescued with VCNs >0.6. This indicated that this limited amount of integrated copies of *ALAS2* was insufficient to prevent the development of the *Alas2*-KO erythroid cells and could not support the generation of sufficient RBCs to reverse the anemia. Conversely, all animals with VCN exceeding 0.6 were successfully reverted from the severe anemic phenotype, a recovery sustained at the 25 weeks after BMT preestablished end point. Only animals treated with X-ALAS2-LV showed high levels of *ALAS2* expression (Figure 1E), and we also observed a direct correlation between VCN and Hb levels (Figure 1F).

X-ALAS2 significantly improves the IE and iron overload of the Alas2-KO^{BM} mice

X-ALAS2-LV treated mice with VCN >0.6 exhibited increased levels of Hb and HCT, improved RBC count, and reticulocyte levels (Figure 3A; Table 1), averaging levels comparable with what would be considered transfusion-free survival in humans. Both treated models showed a decreased expansion of the polychromatic erythroid (P3) population and an increased number of RBCs (P5) (Figure 4C; supplemental Figure 2A). RBCs of treated mice were also morphologically more similar to WT (Figure 3D).

Animals treated with X-ALAS2-LV had improved spleen/body weight ratio. Their spleen color and consistency were comparable to WT mice (Figure 4A). The histologic analysis further supported these findings, where the spleens showed improved tissue architecture and definition between red and white pulp (Figure 4B). Additionally, no iron was detected in the liver or the BM (Figures 4C, 5A). The amount of iron in the spleen was similar to control animals, indicating improved iron metabolism (Figures 4B, 5A). Moreover, no iron accumulation was detected in the mitochondria of the animals treated with X-ALAS2-LV (Figure 5C). Animals treated with X-ALAS2-LV also showed an

Figure 4 (continued) and Prussian blue staining in spleen tissues were collected at the end point of each experimental group. Magnification ×10. (C) Representative images of H&E and Prussian blue staining in the bone marrow and liver tissues were collected at the end point of each experimental group. Magnification ×4.

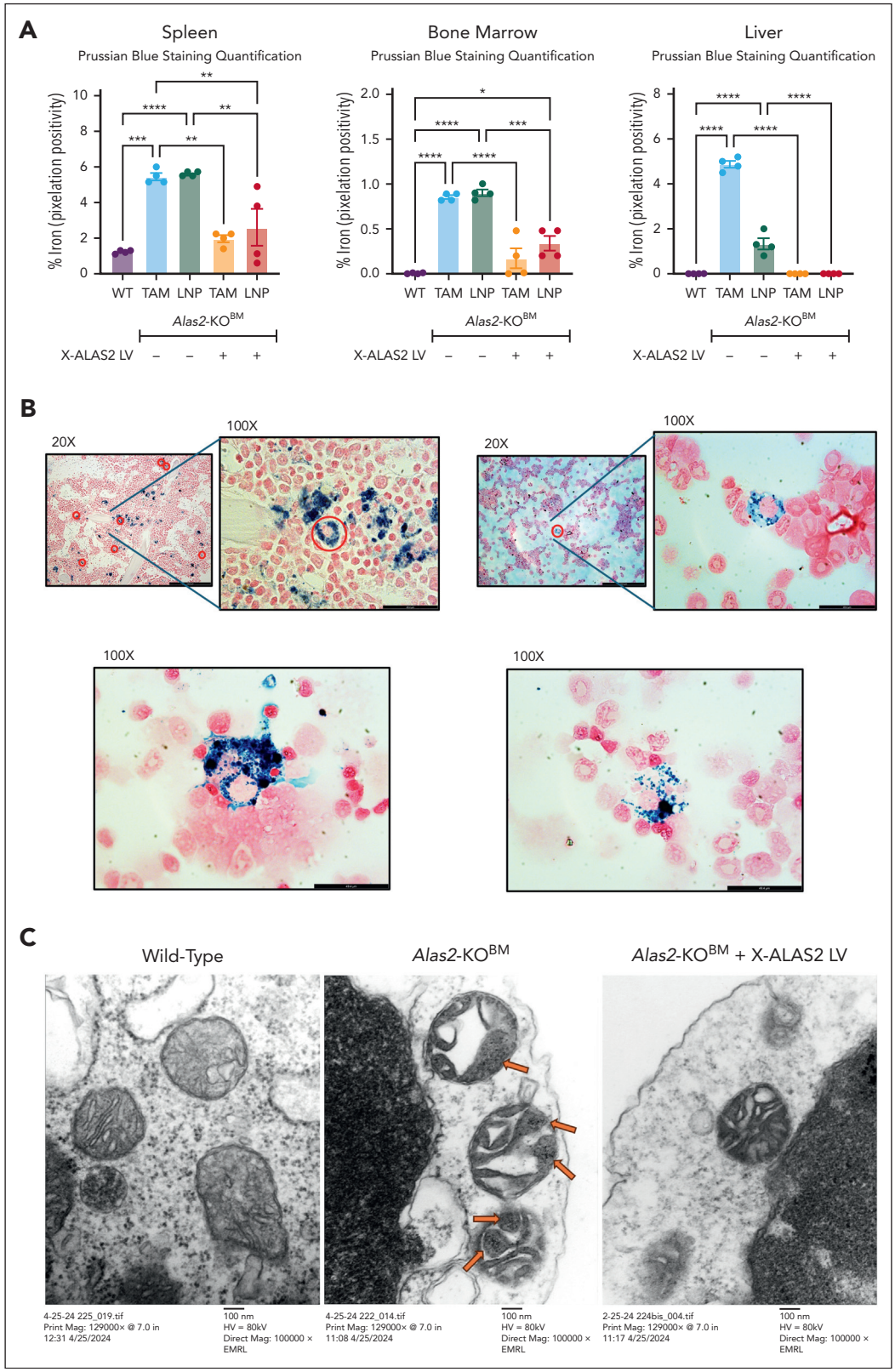

Figure 5. Spleen, bone marrow and liver iron quantification with clear formation of ring sideroblasts and iron accumulation in the mitochondria. (A) Quantification of iron accumulation using the Aperio Versa 200 slide scanner and a positive pixel count algorithm to quantify the level of iron accumulation in the different organs. Data are shown as mean ± standard error of the mean (SEM). *P* values are determined by the Tukey multiple-comparison test after 1-way analysis of variance (ANOVA). **P* < .05, ***P* < .01, ****P* < .001, *****P* < .0001. (B) Representative images of Prussian blue staining in bone marrow tissues and cell smears. Magnifications ×20 and ×100. (C) Representative electron microscopy images of isolated P3 cells from wild type, *Alas2*-KO^{BM}, and X-ALAS2–treated animals. Iron deposits in the mitochondria are highlighted by the orange arrows. Direct magnification is ×100 000 and printed magnification is ×129 000 at 7.0 in.

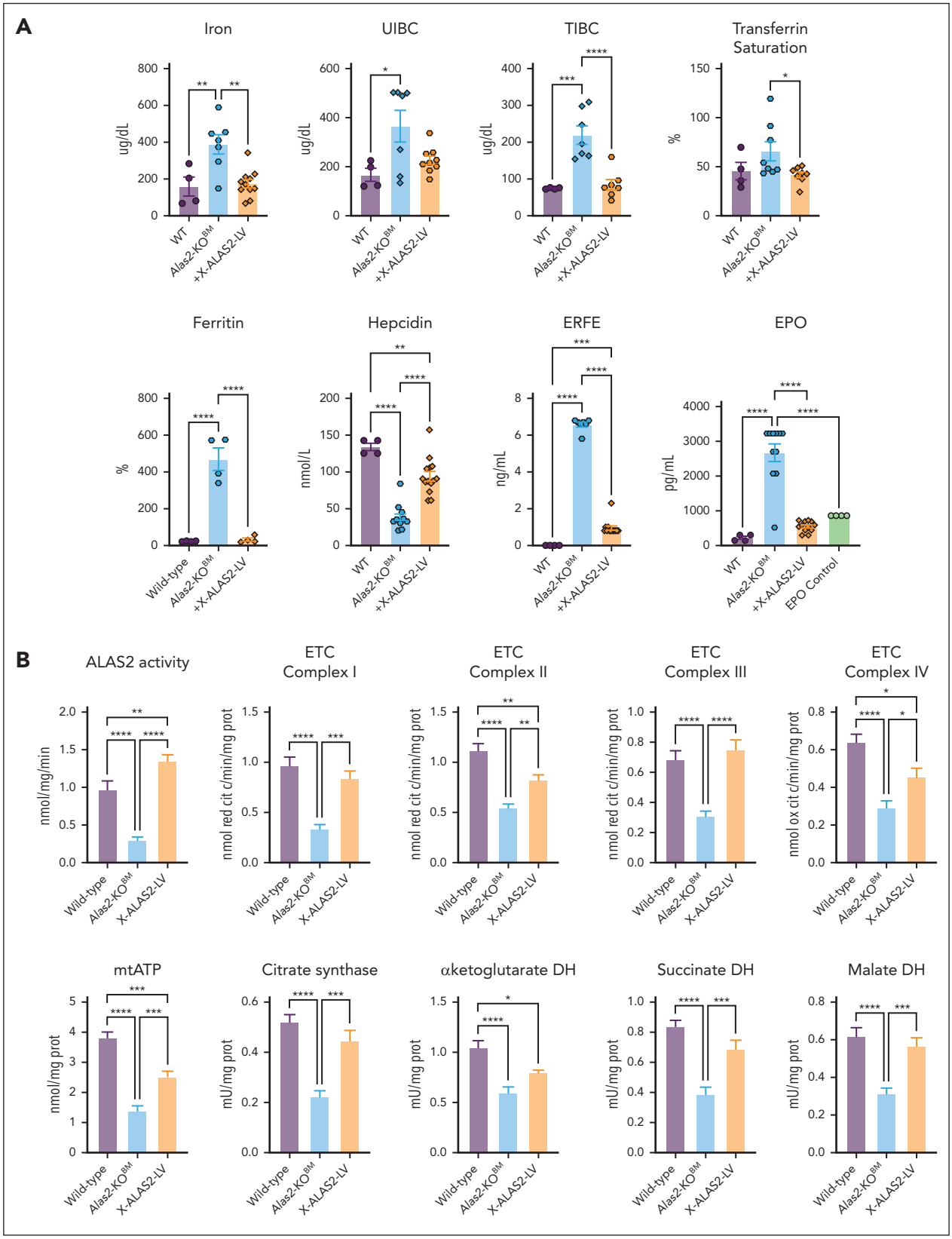

Figure 6. Iron metabolism and metabolomic analysis of the *Alas2*-KO^{BM} model in presence or absence of X-ALAS2-LV. (A) ERFE, HAMP, EPO, and iron values in blood serum of *Alas2*-KO^{BM} animals transduced or not with +/− X-ALAS2-LV at the end point of each experimental group (N = 4-9 in all experimental groups). Data are shown as mean ± standard error of the mean (SEM). *P* values are determined by the Tukey multiple-comparison test after the 1-way analysis of variance (ANOVA). **P* < .05, ***P* < .01, ****P* < .001, *****P* < .0001. WT is a C57BL/6J used as a reference. (B) Metabolomic analysis of polychromatic erythroid cells, sorted from WT and *Alas2*-KO^{BM} animals (N = 6 for each group). Data are shown as mean ± SEM. *P* values are determined by the Tukey multiple-comparison test after the 1-way ANOVA. **P* < .05, ***P* < .01, ****P* < .001, *****P* < .0001. (C) Glycolysis analysis of polychromatic erythroid cells, sorted from WT and *Alas2*-KO^{BM} animals (N = 6 for each group). Data are shown as mean ± SEM. *P* values are

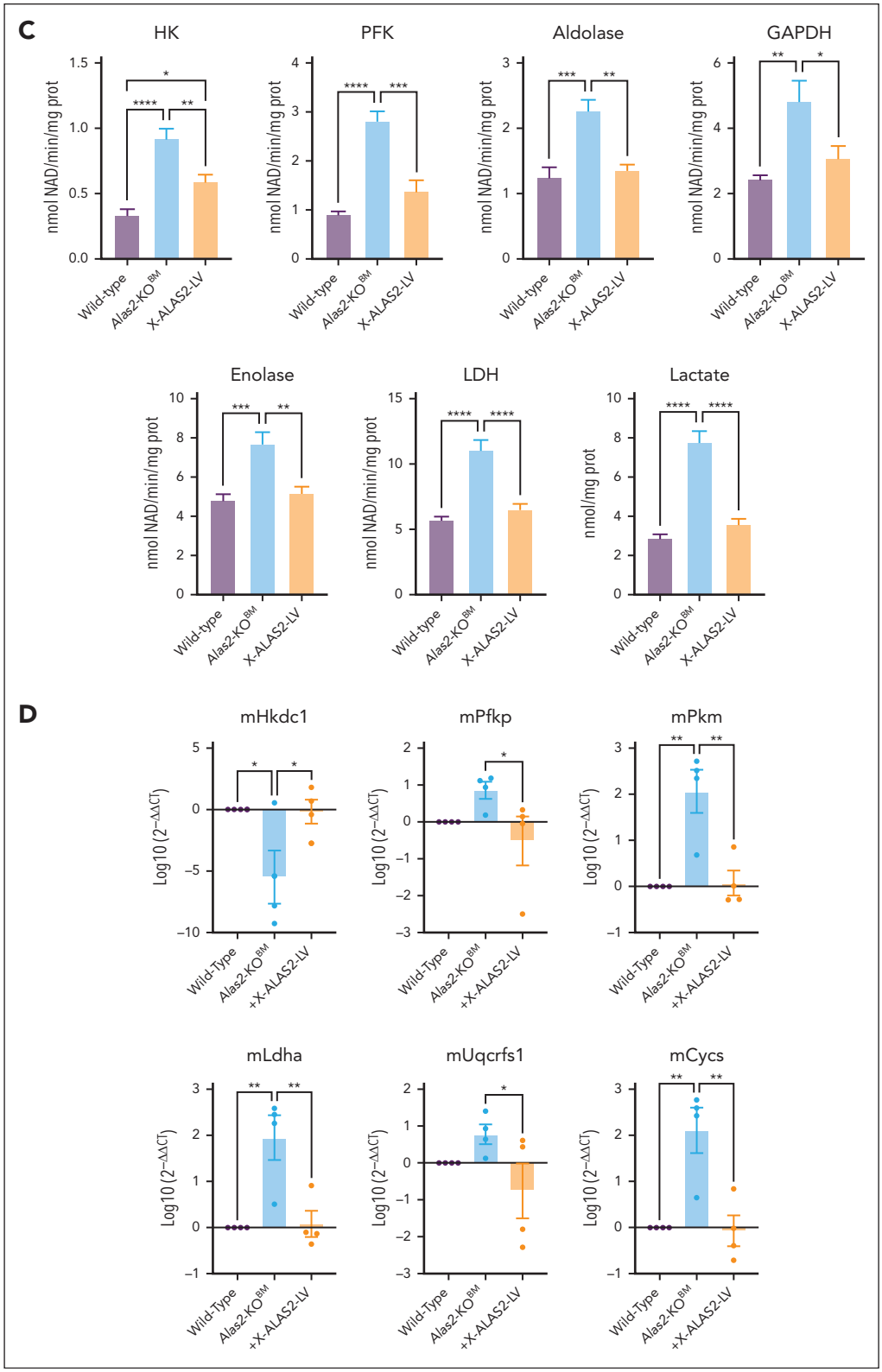

Figure 6 (continued) determined by the Tukey multiple-comparison test after the 1-way ANOVA. *P < .05, **P < .01, ***P < .001, ****P < .0001. (D) Relative gene expression analysis of glycolytic pathway (quantitative reverse transcription polymerase chain reaction [qRT-PCR]) in polychromatic erythroid cells, sorted from WT and *Alas2*-KO^{BM} animals (N = 6 for each group). P values are determined by the Tukey multiple-comparison test after the 1-way ANOVA. *P < .05, **P < .01.

improved iron metabolism, trending closer to the parameters in WT animals (Figure 6A). The mitochondrial and glycolytic metabolism in the treated animals showed improvement toward the WT phenotype (Figure 6B-C). Interestingly, although the expression of glycolytic enzymes aligned with the restored activity, the transcriptional levels of specific critical components

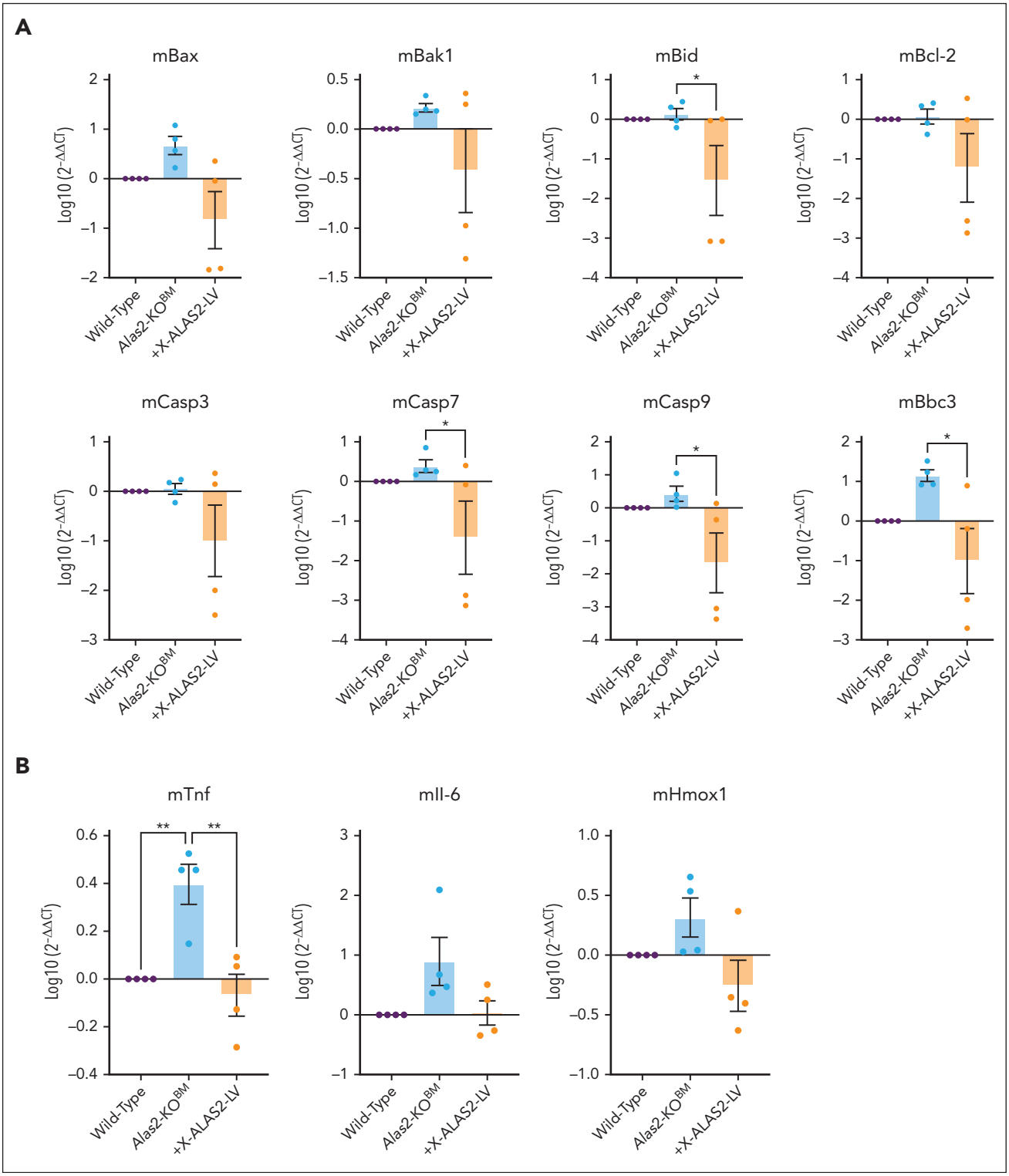

Figure 7. Apoptosis and inflammation gene expression analysis in the *Alas2*-KO^{BM} model and effect of the treatment with X-ALAS2-LV. (A) Relative gene expression analysis of apoptosis pathway (quantitative reverse transcription polymerase chain reaction [qRT-PCR]) in polychromatic erythroid cells, sorted from WT and *Alas2*-KO^{BM} animals (N = 6 for each group). *P* values are determined by the Tukey multiple-comparison test after the 1-way analysis of variance (ANOVA). **P* < .05. (B) Relative gene expression analysis of *Tnf, mIl-6,* and *Hmox1* (qRT-PCR) in polychromatic erythroid cells, sorted from WT and *Alas2*-KO^{BM} animals (N = 6 for each group). *P* values are determined by the Tukey multiple-comparison test after the 1-way ANOVA. ***P* < .01.

of the electron transport chain did not match their enzymatic activity, likely indicating specific and different compensatory responses to changes in metabolism (Figure 6D). Nevertheless, a sensible improvement in the shape and area of the mitochondrial cristae was observed (supplemental Figure 4). The animals also exhibited a decreased expression of proapoptotic

and inflammatory genes, as the reintroduction of ALAS2 conferred antiapoptotic and anti-inflammatory effects (Figure 7A-B).

Secondary BMTs confirmed integration of X-ALAS2-LV in long-term HSC. Notably, Hb, RBC, HCT, and reticulocyte levels in secondary recipients were comparable to those of the primary chimeras (supplemental Figure 5A). Additionally, both groups (TAM and LNP cohorts) exhibited stable VCN levels, ranging from 1.2 to 1.4 in the BM at 25 weeks after transplantation (supplemental Figure 5B). Animals showed low levels of endogenous *Alas2*, indicating that their survival was due to the activity of X-ALAS2-LV (supplemental Figure 5C). Secondary recipients showed improved and effective erythropoiesis and RBC production comparable to WT animals (supplemental Figure 5D). These results highlight the persistent correction of the *Alas2-KO*^{BM} phenotype over time.

Discussion

This study characterized the pathophysiology of a new murine model of XLSA and explored the therapeutic potential of ex vivo HSC gene therapy using a novel lentiviral vector expressing the human *ALAS2* gene. In contrast to our murine model, patients affected by XLSA usually carry missense mutations or in regulatory regions with partial loss of function or decreased *ALAS2* expression, respectively.[1,16,17,44-47] In fact, except for nonsense mutations in clinically affected female carriers, in families with lethal *ALAS2* mutations, no affected males were generally identified in the pedigree.[11] In general, patients are male and become symptomatic at variable ages and typically before the age of 40 years.[17,48,49] XLSA is usually a relatively late-onset disease, whereas our model recapitulates this disorder's most rapid and severe hypothetical form. Therefore, it anticipates that a vector that rescues a more severe disease model will be curative in patients with some ALAS2 activity.

To generate a severe *Alas2*-KO model, we successfully induced the deletion of the murine *Alas2* gene using 2 independent approaches. Our findings demonstrated comparable phenotypes between the TAM and LNP-induced models. However, targeted LNP encapsulating mRNA encoding the Cre recombinase was superior to TAM treatment (Figure 2D), having the advantage of inducing a more rapid and efficient *Alas2* deletion. This underscores the potential of targeted LNP-mediated Cre-mRNA delivery as an effective method for accelerating the study of hematological phenotypes and diseases.

Irrespective of the approach used, our study's significant findings include establishing a robust anemic phenotype in mice through induced *Alas2* gene deletion, characterized by reduced Hb levels, diminished RBC count, IE, and ring sideroblast formation. Interestingly, this is the first study, to our knowledge, elucidating the importance of ALAS2 in the polychromatic erythroblast population, highlighting the step of erythroid development in which ALAS2 activity and heme synthesis are most required. The lack of ALAS2 in this population was associated with an expansion in the number of cells at this stage of differentiation, with a high proportion of cells undergoing cell death. Importantly, within these cells, we observed significantly defective function in the electron transport chain, resulting in low levels of mtATP. The intriguing hypothesis is that the diminished oxidative metabolism in the P3 population might be responsible for the hindered differentiation and maturation into orthochromatic cells. Indeed, it is well established that HSCs, committed progenitors, and fully differentiated blood cells exhibit significant differences in their metabolic characteristics and mitochondrial functions and that alterations in mitochondrial metabolism and activity are not merely passive consequences but active drivers of progenitors' fate decisions.[50,51] More precisely, previous research has suggested that mitochondrial function and oxidative phosphorylation are critical in sustaining the terminal phases of erythroid differentiation.[52] Finally, these findings are consistent with prior studies that have elucidated the importance of heme synthesis in triggering metabolic rewiring in various nonerythroid tissues.[53,54] Furthermore, our study showed a strong correlation between anemia and altered iron metabolism, as it has also been reported in a few patients with XLSA in the absence of blood transfusions.[55] In our mice, we observed that expansion in the polychromatic erythroblast population was associated with high ERFE levels, likely responsible for low HAMP synthesis. The histologic analysis provided further insights, revealing consistent alterations in the liver, spleen, and BM of *Alas2*-KO^{BM} mice, including extramedullary hematopoiesis and iron accumulation. This mouse model, together with the transgenic lines recently described by Ducamp et al, provides a comprehensive view of XLSA, capturing the cellular and physiological effects and enabling therapeutic intervention studies.[56] Previously described human cell lines offer detailed insights into cellular mechanisms specific to human erythropoiesis, but they lack the ability to model the disease's systemic consequences.[57,58] Together, these models provide complementary value: the mouse model is more suitable for studying overall disease progression and therapy, whereas the human cell lines are ideal for investigating specific human cellular responses.

We also showed that X-ALAS2-LV can improve the fatal anemia caused by the complete KO of the *Alas2* gene. Treatment with X-ALAS2-LV extended the survival of animals with VCN <0.6, although these mice eventually showed progressive anemia that required their sacrifice. In animals with VCN >0.6 instead, treatment with X-ALAS2-LV improved the disease phenotype, leading to medium-high levels of Hb synthesis (proportional to VCN), improved splenomegaly, and extramedullary hematopoiesis. These animals also presented improved glycolysis and mitochondrial activity. In animals with lower VCN, a good proportion of cells were likely still generating erythroid cells with no ALAS2 activity, limiting the therapeutic potential of X-ALAS2-LV. Another possibility is that the human ALAS2 may not be as efficient as the mouse orthologue, hindering the therapeutic potential of X-ALAS2-LV in mice. Nevertheless, in animals with VCN >0.6, the improvement of the iron metabolism, coupled with improved complete blood cell levels, highlighted the therapeutic effect of X-ALAS2-LV in ameliorating both erythropoiesis and iron homeostasis, prominent features of XLSA. Notably, animals treated with X-ALAS2-LV showed VCN in the range of 0.6 to 1.4, indicating that a relatively small number of integrations were sufficient to improve *Alas2*-KO^{BM} animals. These findings suggest that HSCs carrying relatively low VCN of X-ALAS2-LV could be curative in patients with XLSA who exhibit hypomorphic or residual expression of the *ALAS2* gene.

Acknowledgments

The authors thank the Flow Cytometry Core Laboratory at the Children's Hospital of Philadelphia, directed by Florin Tuluc, for refining the sorting technique to obtain the polychromatic erythroid populations. The authors also acknowledge the expertise of the Electron Microscopy Core team at the University of Pennsylvania for providing high-quality images and supporting this article.

This study was supported by the Frontier Program (The Children's Hospital of Philadelphia), Comprehensive Center for the Cure of Sickle Cell Disease and Other Red Cell Disorders (GRT-00001923-05), Commonwealth Universal Research Enhancement Program, Pennsylvania Department of Health, Penn Institute for Regenerative Medicine grant (GRT-0000399), National Institutes of Health/National Institute of Diabetes and Digestive and Kidney Diseases (R01 DK095112 and R01 DK133475) to S.R.; and Italian Association for Cancer Research grants IG 24922 (to E.T.) and IG21480 (to C.R.). The veterinary pathologists performing the histopathologic analysis are part of the University of Pennsylvania Penn Vet Comparative Pathology Core Facility (RRID: SCR_022438) and are supported by the Abramson Cancer Center Support grant (P30 CA016520). The scanner used for whole slide imaging and the image analysis software was supported by a National Institutes of Health Shared Instrumentation grant (S12 OD023465-01A1).

Authorship

Contribution: C.C.C. made the experiments and wrote the manuscript; L.B. and A.G. supported the data analysis and the preparation of the manuscript; H.P., B.L.M., Y.K.T., and T.E.P. provided the targeted lipid nanoparticles; E.R., C.-A.A., and G.F. performed the pathology evaluation; E.T., V.F., S.P., S.F., and C.R. performed some experiments; and S.R. designed the experiment and wrote the manuscript.

Conflict-of-interest disclosure: S.R. is a scientific advisory board member of Ionis Pharmaceuticals, Meira GTx, Vifor, and Disc Medicine. Present to past 5 years: S.R. has been or is a consultant for Glaxo-SmithKline, Bristol Myers Squibb, Incyte, Cambridge Healthcare Res, Celgene Corporation, Catenion, First Manhattan Co, FORMA Therapeutics, Ghost Tree Capital, Keros Therapeutics, Noble insight, Protagonist Therapeutics, Sanofi Aventis U.S., Slingshot Insight, Spexis AG, Techspert.io, BVF Partners L.P., Rallybio, LLC, venBio Select LLC, ExpertConnect LLC, and LifeSci Capital. H.P. is a scientific founder and holds equity in Capstan Therapeutics. Y.K.T. and B.L.M. are employees and hold equity in Acuitas Therapeutics. H.P. receives research support from BioNTech. The remaining authors declare no competing financial interests.

ORCID profiles: C.C.C., 0000-0002-1002-8969; L.B., 0000-0003-2133-4432; T.E.P., 0000-0001-5116-0782; A.G., 0000-0002-6602-1854; E.R., 0000-0002-2885-0221; C.-A.A., 0000-0003-0073-2730; Y.K.T., 0000-0002-4083-5251; S.F., 0009-0005-1657-7650; C.R., 0000-0001-9787-4836; V.F., 0000-0001-9063-7918; S.P., 0000-0002-4349-726X; E.T., 0000-0002-1622-2340; S.R., 0000-0002-0938-6558.

Correspondence: Hamideh Parhiz, Department of Systems Pharmacology and Translational Therapeutics, University of Pennsylvania Perelman School of Medicine, 421 Curie Blvd, Philadelphia, PA 19104; email: hamideh.parhiz@pennmedicine.upenn.edu; and Stefano Rivella, The Children's Hospital of Philadelphia, Abramson Research Center, Division of Hematology, 3615 Civic Center Blvd, Philadelphia, PA 19104; email: rivellas@chop.edu.

Footnotes

Submitted 2 July 2024; accepted 14 August 2024; prepublished online on *Blood* First Edition 10 December 2024. https://doi.org/10.1182/blood.2024025846.

Presented in abstract form at the 66th annual meeting of the American Society of Hematology, San Diego, CA, 7 to 10 December 2024.

For original data, please contact rivellas@chop.edu

The online version of this article contains a data supplement.

There is a *Blood* Commentary on this article in this issue.

The publication costs of this article were defrayed in part by page charge payment. Therefore, and solely to indicate this fact, this article is hereby marked "advertisement" in accordance with 18 USC section 1734.

REFERENCES

1. Fujiwara T, Harigae H. Molecular pathophysiology and genetic mutations in congenital sideroblastic anemia. *Free Radic Biol Med*. 2019;133:179-185.
2. Ducamp S, Fleming MD. The molecular genetics of sideroblastic anemia. *Blood*. 2019;133(1):59-69.
3. Bottomley SS, Fleming MD. Sideroblastic anemia: diagnosis and management. *Hematol Oncol Clin North Am*. 2014;28(4):653-670.
4. Liu J, Li Y, Tong J, et al. Long non-coding RNA-dependent mechanism to regulate heme biosynthesis and erythrocyte development. *Nat Commun*. 2018;9(1):4386.
5. Zhang Y, Zhang J, An W, et al. Intron 1 GATA site enhances ALAS2 expression indispensably during erythroid differentiation. *Nucleic Acids Res*. 2017;45(2):657-671.
6. Khechaduri A, Bayeva M, Chang HC, Ardehali H. Heme levels are increased in human failing hearts. *J Am Coll Cardiol*. 2013;61(18):1884-1893.
7. Ohba R, Furuyama K, Yoshida K, et al. Clinical and genetic characteristics of congenital sideroblastic anemia: comparison with myelodysplastic syndrome with ring sideroblast (MDS-RS). *Ann Hematol*. 2013;92(1):1-9.
8. Cotter PD, May A, Fitzsimons EJ, et al. Late-onset X-linked sideroblastic anemia: missense mutations in the erythroid delta-aminolevulinate synthase (ALAS2) gene in two pyridoxine-responsive patients initially diagnosed with acquired refractory anemia and ringed sideroblasts. *J Clin Invest*. 1995;96(4):2090-2096.
9. Cazzola M, May A, Bergamaschi G, Cerani P, Rosti V, Bishop DF. Familial-skewed X-chromosome inactivation as a predisposing factor for late-onset X-linked sideroblastic anemia in carrier females. *Blood*. 2000;96(13):4363-4365.
10. Aivado M, Gattermann N, Rong A, et al. X-linked sideroblastic anemia associated with a novel ALAS2 mutation and unfortunate skewed X-chromosome inactivation patterns. *Blood Cells Mol Dis*. 2006;37(1):40-45.
11. Rose C, Callebaut I, Pascal L, et al. Lethal ALAS2 mutation in males X-linked sideroblastic anaemia. *Br J Haematol*. 2017;178(4):648-651.
12. Ducamp S, Kannengiesser C, Touati M, et al. Sideroblastic anemia: molecular analysis of the ALAS2 gene in a series of 29 probands and functional studies of 10 missense mutations. *Hum Mutat*. 2011;32(6):590-597.
13. Katsurada T, Kawabata H, Kawabata D, et al. A Japanese family with X-linked sideroblastic anemia affecting females and manifesting as macrocytic anemia. *Int J Hematol*. 2016;103(6):713-717.
14. Morimoto Y, Chonabayashi K, Kawabata H, et al. Azacitidine is a potential therapeutic drug for pyridoxine-refractory female X-linked sideroblastic anemia. *Blood Adv*. 2022;6(4):1100-1114.
15. Yoshida K, Sanada M, Shiraishi Y, et al. Frequent pathway mutations of splicing machinery in myelodysplasia. *Nature*. 2011;478(7367):64-69.
16. Bekri S, May A, Cotter PD, et al. A promoter mutation in the erythroid-specific 5-aminolevulinate synthase (ALAS2) gene causes X-linked sideroblastic anemia. *Blood*. 2003;102(2):698-704.
17. Kaneko K, Furuyama K, Fujiwara T, et al. Identification of a novel erythroid-specific enhancer for the ALAS2 gene and its loss-of-function mutation which is associated with congenital sideroblastic anemia. *Haematologica*. 2014;99(2):252-261.
18. Astner I, Schulze JO, van den Heuvel J, Jahn D, Schubert WD, Heinz DW. Crystal

structure of 5-aminolevulinate synthase, the first enzyme of heme biosynthesis, and its link to XLSA in humans. *EMBO J*. 2005;24(18):3166-3177.

19. May A, Bishop DF. The molecular biology and pyridoxine responsiveness of X-linked sideroblastic anaemia. *Haematologica*. 1998;83(1):56-70.
20. Ishida H, Imamura T, Morimoto A, Fujiwara T, Harigae H. Five-aminolevulinic acid: new approach for congenital sideroblastic anemia. *Pediatr Int*. 2018;60(5):496-497.
21. Cavazzana-Calvo M, Payen E, Negre O, et al. Transfusion independence and HMGA2 activation after gene therapy of human beta-thalassaemia. *Nature*. 2010;467(7313):318-322.
22. Negre O, Eggimann AV, Beuzard Y, et al. Gene therapy of the beta-hemoglobinopathies by lentiviral transfer of the beta(A(T87Q))-globin gene. *Hum Gene Ther*. 2016;27(2):148-165.
23. Miccio A, Cesari R, Lotti F, et al. In vivo selection of genetically modified erythroblastic progenitors leads to long-term correction of beta-thalassemia. *Proc Natl Acad Sci U S A*. 2008;105(30):10547-10552.
24. Negre O, Bartholomae C, Beuzard Y, et al. Preclinical evaluation of efficacy and safety of an improved lentiviral vector for the treatment of beta-thalassemia and sickle cell disease. *Curr Gene Ther*. 2015;15(1):64-81.
25. Boulad F, Wang X, Qu J, et al. Safe mobilization of CD34+ cells in adults with beta-thalassemia and validation of effective globin gene transfer for clinical investigation. *Blood*. 2014;123(10):1483-1486.
26. Breda L, Ghiaccio V, Tanaka N, et al. Lentiviral vector ALS20 yields high hemoglobin levels with low genomic integrations for treatment of beta-globinopathies. *Mol Ther*. 2021;29(4):1625-1638.
27. Nakajima O, Takahashi S, Harigae H, et al. Heme deficiency in erythroid lineage causes differentiation arrest and cytoplasmic iron overload. *EMBO J*. 1999;18(22):6282-6289.
28. Peoc'h K, Nicolas G, Schmitt C, et al. Regulation and tissue-specific expression of delta-aminolevulinic acid synthases in non-syndromic sideroblastic anemias and porphyrias. *Mol Genet Metab*. 2019;128(3):190-197.
29. Feil S, Valtcheva N, Feil R. Inducible Cre mice. *Methods Mol Biol*. 2009;530:343-363.
30. Breda L, Papp TE, Triebwasser MP, et al. In vivo hematopoietic stem cell modification by mRNA delivery. *Science*. 2023;381(6656):436-443.
31. Liu J, Zhang J, Ginzburg Y, et al. Quantitative analysis of murine terminal erythroid differentiation in vivo: novel method to study normal and disordered erythropoiesis. *Blood*. 2013;121(8):e43-e49.
32. Richard C, Verdier F. Transferrin receptors in erythropoiesis. *Int J Mol Sci*. 2020;21(24):9713.
33. Guerra A, Parhiz H, Rivella S. Novel potential therapeutics to modify iron metabolism and red cell synthesis in diseases associated with defective erythropoiesis. *Haematologica*. 2023;108(10):2582-2593.
34. Cogliati S, Enriquez JA, Scorrano L. Mitochondrial cristae: where beauty meets functionality. *Trends Biochem Sci*. 2016;41(3):261-273.
35. Breda L, Casu C, Gardenghi S, et al. Therapeutic hemoglobin levels after gene transfer in beta-thalassemia mice and in hematopoietic cells of beta-thalassemia and sickle cells disease patients. *PLoS One*. 2012;7(3):e32345.
36. Roselli EA, Mezzadra R, Frittoli MC, et al. Correction of beta-thalassemia major by gene transfer in haematopoietic progenitors of pediatric patients. *EMBO Mol Med*. 2010;2(8):315-328.
37. Romero Z, Campo-Fernandez B, Wherley J, et al. The human ankyrin 1 promoter insulator sustains gene expression in a beta-globin lentiviral vector in hematopoietic stem cells. *Mol Ther Methods Clin Dev*. 2015;2:15012.
38. Burgess DJ. Gene therapy: insulating from genotoxicity. *Nat Rev Genet*. 2015;16(3):130-131.
39. Rivella S, Sadelain M. Genetic treatment of severe hemoglobinopathies: the combat against transgene variegation and transgene silencing. *Semin Hematol*. 1998;35(2):112-125.
40. Browning DL, Trobridge GD. Insulators to improve the safety of retroviral vectors for HIV gene therapy. *Biomedicines*. 2016;4(1):4.
41. Zhou X, Liu Q, Wang D, Zhang X, Emery DW, Li CL. The cHS4 chromatin insulator reduces the rate of retroviral vector-mediated gene dysregulation associated with aberrant vector transcription. *Cytogenet Genome Res*. 2017;151(2):72-81.
42. Goodman MA, Arumugam P, Pillis DM, et al. Foamy virus vector carries a strong insulator in its long terminal repeat which reduces its genotoxic potential. *J Virol*. 2018;92(1):e01639-17.
43. Rivella S, Callegari JA, May C, Tan CW, Sadelain M. The cHS4 insulator increases the probability of retroviral expression at random chromosomal integration sites. *J Virol*. 2000;74(10):4679-4687.
44. Camaschella C. Hereditary sideroblastic anemias: pathophysiology, diagnosis, and treatment. *Semin Hematol*. 2009;46(4):371-377.
45. Furuyama K, Sassa S. Multiple mechanisms for hereditary sideroblastic anemia. *Cell Mol Biol (Noisy-le-grand)*. 2002;48(1):5-10.
46. Bergmann AK, Campagna DR, McLoughlin EM, et al. Systematic molecular genetic analysis of congenital sideroblastic anemia: evidence for genetic heterogeneity and identification of novel mutations. *Pediatr Blood Cancer*. 2010;54(2):273-278.
47. Camaschella C. Recent advances in the understanding of inherited sideroblastic anaemia. *Br J Haematol*. 2008;143(1):27-38.
48. Fleming MD. Congenital sideroblastic anemias: iron and heme lost in mitochondrial translation. *Hematology Am Soc Hematol Educ Program*. 2011;2011:525-531.
49. Furuyama K, Harigae H, Kinoshita C, et al. Late-onset X-linked sideroblastic anemia following hemodialysis. *Blood*. 2003;101(11):4623-4624.
50. Papa L, Djedaini M, Hoffman R. Mitochondrial role in stemness and differentiation of hematopoietic stem cells. *Stem Cells Int*. 2019;2019:4067162.
51. Vannini N, Girotra M, Naveiras O, et al. Specification of haematopoietic stem cell fate via modulation of mitochondrial activity. *Nat Commun*. 2016;7:13125.
52. Sen T, Jain M, Gram M, et al. Enhancing mitochondrial function in vivo rescues MDS-like anemia induced by pRb deficiency. *Exp Hematol*. 2020;88:28-41.
53. Fiorito V, Allocco AL, Petrillo S, et al. The heme synthesis-export system regulates the tricarboxylic acid cycle flux and oxidative phosphorylation. *Cell Rep*. 2021;35(11):109252.
54. Petrillo S, De Giorgio F, Kopecka J, et al. Endothelial heme dynamics drive cancer cell metabolism by shaping the tumor microenvironment. *Biomedicines*. 2021;9(11):1557.
55. Lira Zidanes A, Marchi G, Busti F, et al. A novel ALAS2 missense mutation in two brothers with iron overload and associated alterations in serum hepcidin/erythroferrone levels. *Front Physiol*. 2020;11:581386.
56. Ducamp S, Sendamarai A, Campagna DR, et al. Murine models of erythroid 5ALA synthesis disorders and their conditional synthetic lethal dependency on pyridoxine. *Blood*. 2024;144(13):1418-1432.
57. Ono K, Fujiwara T, Saito K, et al. Congenital sideroblastic anemia model due to ALAS2 mutation is susceptible to ferroptosis. *Sci Rep*. 2022;12(1):9024.
58. Kaneko K, Kubota Y, Nomura K, et al. Establishment of a cell model of X-linked sideroblastic anemia using genome editing. *Exp Hematol*. 2018;65:57-68.e2.

An erythroid-specific lentiviral vector improves anemia and iron metabolism in a new model of XLSA.

Supplementary Materials

This file includes:

MATERIALS AND METHODS

Institutional Animal Care and Use Committee (IACUC) regulation.

All experiments performed in mice were approved by the IACUC (protocol #1173) at the Children's Hospital of Philadelphia. The animals have been housed in the Children's Hospital of Philadelphia animal facility according to the standards provided by the OLAW (PHS Animal Welfare Assurance # D16-00280 (A3442-01)) and AAALAC (AAALAC Unit # 000427).

Mouse screening.

The genotyping primers to identify the LoxP sites and the R26-CreER^{T2} sequence are shown in **Tab.S1**.

Cell sorting for isolation of polychromatic erythroid population.

Bone marrow cells extracted from one femur have been washed in 1X PBS. Subsequently, Ter119^{+} cells selection was obtained using MACS LS Columns (Cat. 130-042-401) and Anti-Ter119 Microbeads (Cat. 130-042-401) (Miltenyi Biotec, Auburn, CA). Isolated Ter119^{+} cells were then incubated with FITC anti-mouse Ter-119 (116206) and APC anti-mouse/human CD44 (103012) antibodies and Propidium Iodide (PI) (421301) (Biolegend, San Diego, CA) and polychromatic erythroid population (P3) was sorted using a BD FACSMelody™ Cell Sorter and BD FACSChorus software (BD Biosciences, Franklin Lakes, NJ), using a 100µm nozzle at 23 PSI, drop frequency 34 kHz. P3 sorted cells were centrifuged at 400xg for 5 minutes at 4°C and immediately frozen and stored at -80°C until processing for analysis.

Mitochondria isolation

As described in Xu X. et al.[1], cells were washed twice in ice-cold 0.1M phosphate-buffered saline (PBS), then lysed in 0.5mL buffer A (50 mM Tris-HCl, 100 mM KCl, 5 mM $MgCl_2$, 1.8 mM ATP, 1 mM EDTA, pH 7.2), supplemented with protease inhibitor cocktail III (Merck KGaA, Darmstadt, DE, containing 100 mmol/L AEBSF, 80mmol/L aprotinin, 5mmol/L bestatin, 1.5mmol/L E-64, 2mmol/L leupeptin, and 1mmol/L pepstatin), 1 mM phenylmethylsulfonyl

fluoride (PMSF), 250 mM NaF. Samples were clarified by centrifuging at 650 *g* for 3 minutes at 4°C. Supernatants were collected and centrifuged at 13,000 *g* for 5 minutes at 4°C. The new supernatants were discarded. Pellets containing mitochondria were washed once with 0.5mL buffer A and re-suspended in 0.25mL buffer B (250 mM sucrose, 15 mM K_2HPO_4, 2 mM $MgCl_2$, 0.5 mM EDTA, 5% w/v bovine serum albumin). A 50 µL aliquot was sonicated to measure protein content with the BCA Protein Assay Kit (Sigma Aldrich, St. Louis, MO, USA). To confirm the presence of mitochondrial proteins in the extracts, 10 µg of each sonicated sample were subjected to SDS-PAGE and probed with an anti-porin antibody (Abcam, Cambridge, UK, catalog n° ab14734, clone 20B12AF2). The sonicated samples were used to measure the enzymatic activities of 5'-Aminolevulinate synthase, citrate synthase, α-ketoglutarate dehydrogenase, succinate dehydrogenase, and malate dehydrogenase. The remaining not-sonicated part was used to measure the electron transport chain (ETC) complexes I-IV activities.

Citrate synthase, α-ketoglutarate dehydrogenase, succinate dehydrogenase, and malate dehydrogenase activities

The enzymatic activities of citrate synthase, α-ketoglutarate dehydrogenase, succinate dehydrogenase and malate dehydrogenase were measured on 10µg mitochondrial proteins using the Citrate Synthase Assay Kit (Sigma Aldrich, St. Louis, MO USA, catalog n° MAK193), α-Ketoglutarate Dehydrogenase Activity Assay Kit (Abcam, Cambridge, UK, catalog n° ab185440), Malate Dehydrogenase Assay Kit (Sigma Aldrich, St. Louis, MO USA, catalog n° MAK196), Succinate Dehydrogenase Activity Colorimetric Assay Kit (BioVision, Milpitas, CA USA, catalog n° K660), as per manufacturer's instructions.

Activity of mitochondrial ETC complexes I-IV

The activity of mitochondrial electron transport chain complexes was measured according to Xu X. et al.[1]. Specifically, to measure complex I activity, 20 µg of non-sonicated mitochondrial samples were re-suspended in 0.2 ml buffer 1A (5 mM KH_2PO_4, 5 mM $MgCl_2$, 5% w/v bovine serum albumin), incubated 1 min at RT followed by 7 min in 0.1 ml buffer 1B (25% w/v saponin, 50 mM KH_2PO_4, 5 mM $MgCl_2$, 5% w/v bovine serum albumin, 0.12 mM oxidized ubiquinone, which acts as electrons shuttle from complex I to complex III, 2.5 mM antimycin A, which inhibits complex III, 0.2 mM NaN_3, which blocks complex IV; pH 7.5). 1.5 mM NADH, as an electron donor, was added to the mix. The rate of NADH oxidation was followed for 5 min at 37°C, reading the absorbance at 340 nm. The results were expressed as NAD+ /min/mg mitochondrial protein nanomoles. Complex II activity was measured as the electron transfer rate between complex II and III. 20 µg of non-sonicated mitochondrial samples was re-suspended in 0.1 ml buffer 2A (50 mM KH_2PO_4, 7.5 mM $MgCl_2$, 25% w/v saponin, 20 mM succinic acid; pH 7.2) and incubated for 30 min at room temperature. 0.2 ml buffer 2B (50 mM KH_2PO_4, 7.5 mM $MgCl_2$, 5% w/v bovine serum albumin, 30 mM succinic acid as substrate of complex II, 0.12 mM oxidized ubiquinone as electrons shuttle from complex II to complex III, 0.12 mM oxidized cytochrome c as acceptor of electrons flowing from complex II to complex III, 5 mM rotenone to prevent electron flux from

complex I, 0.2 mM NaN_3, to block complex IV) was added. The reduction rate of cytochrome c was measured for 5 min at 37°C, reading the absorbance at 550 nm. The results were expressed as nanomoles of reduced cytochrome c/min/mg mitochondrial proteins.

The activity of complex III was measured in 50 µg of non-sonicated mitochondrial samples re-suspended in 0.2 ml buffer A (5 mM KH_2PO_4, 5 mM $MgCl_2$, 5% w/v bovine serum albumin, bovine serum albumin; pH 7.2) to which 0.1 ml buffer B (25% w/v saponin, 50 mM KH_2PO_4, 5 mM $MgCl_2$, 5% w/v bovine serum albumin, 0.12 mM oxidized cytochrome c, 0.2 mM NaN_3, which blocks complex IV allowing the accumulation of reduced cytochrome c; pH 7.5) was added for 5 min at room temperature. The cytochrome c reduction reaction was started by adding 0.15 mM NADH. After 1 min from the addition of NADH, as an inducer of electron flow, 5 mM rotenone, which blocks the activity of complex I, was added. The reduction rate of cytochrome c, dependent on the activity of complex III only in the presence of rotenone, was followed for 5 min at 37°C, reading the absorbance at 550 nm. The results were expressed as nanomoles of reduced cytochrome c/min/mg mitochondrial proteins.

The rate of oxidation of cytochrome c (reduced form, generated by complex III) was measured to measure the activity of complex IV. 20 µg of non-sonicated mitochondrial samples was resuspended in 0.1 ml buffer 4A (50 mM KH_2PO_4, 20 mM succinic acid, 25% w/v saponin; pH 7.2) and incubated for 30 min at room temperature. 0.2 ml buffer 4B (50 mM KH_2PO_4, 5 mM rotenone, which prevents electron flux from complex I to complex III, 30 mM succinic acid as a substrate of complex II and electrons generator, 0.03 mM reduced cytochrome c as an acceptor of electrons flowing from complex III to complex IV) was added. The oxidation rate of cytochrome c was followed for 5 min at 37°C, reading the absorbance at 550 nm. The results were expressed as nanomoles of oxidized cytochrome c/min/mg mitochondrial proteins.

5'-Aminolevulinate synthase activity

ALAS activity was measured according to Bergonia HA et al.[2] on 10µg mitochondrial proteins. 10 µl of the reaction product were injected into a Waters Acquity ultra-performance liquid chromatography (UPLC), equipped with a binary solvent manager, sample manager, photodiode array detector (PDA), fluorescence detector, column heater, and an Acquity UPLC BEH C18, 1.7 µM, 2.1 × 100 mm column. ALA-derivative was detected by setting the detector with excitation λ = 370 nm and emission λ = 460 nm and the range of the PDA scanner between 210 and 500 nm. The results were converted into nmol/min according to a previously set titration curve and expressed as nmol/min/mg mitochondrial proteins.

ATP levels in mitochondria

ATP levels in mitochondria extracts were assessed by the ATP Bioluminescent Assay Kit (Sigma-Aldrich, St. Louis, MO USA, catalog n° FLAA). ATP was quantified as relative light units (RLU) and converted into nmol ATP/mg mitochondrial proteins, according to the calibration curve previously set.

Glycolytic enzyme activities and intracellular lactate

Cells were washed with fresh medium, detached with trypsin/EDTA, re-suspended at 1 x 10^5 cells/ml in 200 µL of 100 mM TRIS 10 mM/EDTA 1 mM (pH 7.4), and sonicated on ice with two 10 s bursts. Enzymatic activities were measured on 10 µl cell lysates, incubated for 5 min at 37°C. The protein content was measured using the BCA1 kit (Sigma Aldrich, St. Louis, MO USA, catalog n°71285-M). Aldolase and hexokinase (HK) activity were measured using the Aldolase Activity Colorimetric Assay Kit (Bio-Vision, Waltham, MA USA, catalog n°K665) and the Hexokinase Activity Assay kit (Abcam, Cambridge, UK, catalog n° ab136957), respectively. The activity of phosphofructokinase-1 (PFK) was measured spectrophotometrically, as reported in a previous work.[3] The activities of glyceraldehyde 3-phosphate dehydrogenase (GAPDH), enolase, and lactate dehydrogenase (LDH) were measured spectrophotometrically according to previous works.[4,5] For GAPDH, tissue lysate was incubated with 5 mM 3-phosphoglyceric acid, 1 U phosphoglycerate 3-kinase, 5 mM ATP, and 2.5 mM NADH. For enolase, cell lysate was incubated with 10 mM $MgCl_2$, 100 mM KCl, 1 mM 2-phosphoglyceric acid, 0.4 mM ADP, 6.8 U/mL pyruvate kinase (PK), 9.9 U/mL LDH, 0.2 mM NADH. For LDH, cell lysate was incubated with 5 mM NADH and 20 mM pyruvic acid. For all assays of glycolytic enzymes, the activities were monitored by measuring the absorbance variation at 340 nm using a Synergy HTX 96-well microplate reader (Bio-Tek Instruments, Winooski, VT). The kinetics were linear throughout the measurement. To measure the intracellular lactate, 100 µg of whole cell lysates were analyzed using the Lactate Assay Kit (Sigma Aldrich, St. Louis, MO USA, catalog n° MAK-064), as per manufacturer's instructions. The amount of lactate was measured spectrophotometrically at 570 nm with a Synergy HTX 96-well microplate reader.

Bone marrow isolation and Lin^- selection.

Bone marrow cells were extracted from animal femurs employing mechanical crushing to optimize cell recovery. BM cells were then suspended in 4% FBS from Hyclone (Logan, UT) in PBS solution from Gibco (Waltham, MA). Following the manufacturer's guidelines, red blood cells were lysed using ACK lysis buffer from Gibco (Waltham, MA) and filtered through a 40 mM sterile strainer from Corning (Glendale, AZ). Cells were washed with a 4% FBS PBS solution. Following lysis, cell number, and viability were assessed using AOPI staining on a Cellometer Auto 2000 cell viability counter from Nexcelom Bioscience (Lawrence, MA). Cells were seeded at 1.5E+06/mL concentration in Stemspan SFEM from Stem Cell Technologies (Vancouver, BC, Canada). The culture medium was supplemented with 50 ng/mL mSCF, 6 ng/mL mIL-3, and 10 ng/mL mIL-6, all provided by Peprotech (Cranbury, NJ). Lin^- HSCs were isolated by immunobeading using the mouse lineage cell depletion kit (130-110-470) from Miltenyi Biotech (Auburn, CA, USA).

HSCs transduction with LV and transfection with LNP.

1.5E+06/mL Lin^- HSCs isolated from the BM of donor mice (8–12 weeks old) (as described above) were transduced overnight using a range of 100-150 MOI/cell in StemSpan Serum Free Expansion Medium (SFEM) culture medium from StemCell Technologies (Vancouver, Canada). The culture medium was supplemented with 50 ng/mL recombinant murine stem cell factor (mSCF), 10 ng/mL

recombinant murine interleukin-6 (IL-6), 6 ng/mL IL-3 from PeproTech (Rocky Hill, NJ, USA), 200 mM L-glutamine, 100 U/mL penicillin/streptomycin from Gibco (Thermo Fisher Scientific), 0.2 mg/mL Poloxamer 338 from Sigma-Aldrich (St. Louis, MO), and 2 µL/mL Lentiblast Premium from OZ Biosciences (San Diego, CA). For the *Alas2*-KO^{BM} experimental group, BM cells isolated from the femurs of 2 mice (depleted of RBC as described above) were seeded at a concentration of 1.5E+06/mL in Stemspan SFEM from Stem Cell Technologies (Vancouver, BC, Canada). The culture medium was supplemented with 50 ng/mL mSCF, 6 ng/mL mIL-3, and 10 ng/mL mIL-6 and incubated with 1.0µg of the LNP^{CD117}Cre formulation. A fraction of the cells was retained for 24 and 72 hours for analysis of allelic deletion. For the X-ALAS2-LV experimental group, 1.5E+06/mL Lin$^-$ cells were incubated with 1.0µg/1E+06 of LNP^{CD117}Cre for 2 hours, followed by overnight transduction with X-ALAS2 LV using a range of 100-150 MOI/cell.

Bone marrow transplantation.

300,000 viable untreated or treated Lin$^-$ donor cells were injected intravenously into lethally irradiated (two doses of 550cGy each, administered 4 hours apart) B6.SJL-PtprcaPepcb/BoyJ or C57BL/6-Tg(UBC-GFP)30Scha/J recipient mice (8–12 weeks old, sourced from The Jackson Laboratory, Bar Harbor, ME, USA). Cell injections took place at least 1 hour after the second irradiation dose. Secondary transplants were performed by injecting 10^6 whole BM cells into lethally irradiated secondary recipient mice following the same protocol as the primary transplants listed above.

Tamoxifen preparation and administration.

Tamoxifen was purchased by Millipore-Sigma (Burlington, MA, USA) and dispersed in Corn Oil (Millipore-Sigma - Burlington, MA, USA) at the 10 mg/mL stock concentration. A 1 mL syringe with a 21-gauge 5/8 needle was used for IP administration in the lower abdomen of 1mg/mouse. Tamoxifen irradiated chow was purchased by Inotiv (Chicago, IL, USA) at a 500 mg/Kg diet concentration. It has been provided *ad libitum,* considering a daily intake of 80 mg/kg body weight.

RNA synthesis and preparation of targeted LNP-mRNA.

The gene coding sequence for cre recombinase was cloned into an IVT-mRNA production template plasmid containing a T7 promoter, 5' and 3' UTR elements, Kozak consensus sequence, and 101 poly(A) tail. DNA synthesis, cloning, and industrial-grade endotoxin-free plasmid preparation were provided by GenScript (Piscataway, NJ, USA). IVT-mRNA was produced using linearized IVT template plasmid and the MEGAScript T7 kit (Thermo Fisher Scientific, AMB13345, Waltham, MA, USA) and formulated with nucleoside-modified m1Ψ-5'-triphosphate (TriLink, N-1081, San Diego, CA). 5' Capping of the IVT-mRNAs was performed co-transcriptionally using the trinucleotide cap1 analog, CleanCap® Reagent AG (3' OMe) (TriLink, N-7413, San Diego, CA, USA). Single-stranded IVT-mRNA was purified by cellulose purification, as previously described.[6] All mRNAs were analyzed by agarose gel electrophoresis and were stored at -20°C. Cellulose-purified m1Ψ-containing RNAs were encapsulated in LNP

using a self-assembly process as previously described.[7] An ethanolic lipid mixture of ionizable cationic lipid, phosphatidylcholine, cholesterol, and polyethylene glycol-lipid was rapidly mixed with an aqueous solution containing the mRNA at acidic pH. The RNA-loaded particles were characterized by dynamic light scattering using a Zetasizer Nano ZS (Malvern Instruments, Malvern, UK) and a Ribogreen assay. The mean hydrodynamic diameter of these LNP- mRNAs was approximately 80nm with a polydispersity index of 0.02-0.06 and an encapsulation efficiency of ~95%. LNPs used in this study are proprietary to Acuitas Therapeutics (Vancouver, BC, Canada). To prepare antibody-targeted LNP-mRNA, LNP-mRNA were conjugated with purified rat anti-mouse CD117 (c-kit), clone 2B8 (BioLegend, 93235, San Diego, CA, USA) via SATA–maleimide chemistry, as described previously.[8] Briefly, LNPs were modified with maleimide functioning groups (DSPE-PEG-mal) by a post-insertion technique. The antibody was functionalized with SATA (N-succinimidyl S-acetyl thioacetate, 26102) from Thermo Fisher (Burlington, MA, USA) to introduce sulfhydryl groups allowing conjugation to maleimide. SATA was deprotected using 0.5 M hydroxylamine, followed by removal of the unreacted components by Zeba spin desalting columns (Thermo Fisher Scientific, 89890, Waltham, MA, USA). The reactive sulfhydryl group on the antibody was then conjugated to maleimide moieties using thioether conjugation chemistry. Purification was done using Sepharose CL-4B gel filtration columns (MilliporeSigma, GE17-0150-01, Burlington, MA, USA). mRNA content was calculated by performing a modified Quant-iT RiboGreen RNA assay (Thermo Fisher Scientific, R11490, Waltham, MA, USA). After adding the targeting ligand, all the targeted and non-targeted LNP preparations were kept at 4°C and used within three days of preparation.

RAL Diff-Quik Stain.

Peripheral blood smears were created using a drop of freshly collected blood on a standard glass slide. Slides were allowed to air dry and then stained with the RAL Diff-Quik stain (Siemens, Munich, Germany) according to the manufacturer's instructions. Slides were placed in Diff-Quik solution I for 5 seconds, blotted, and placed in Diff-Quik solution II for 5 seconds and in Diff-Quik solution III for 5 seconds before being washed in distilled water and allowed to air dry and imaged using an Olympus BX60 Microscope (EVIDENT, Olympus Scientific Solutions Americas DBA, Waltham, MA) and an Infinity2 Lumenera camera and Lumenera Capture software (Lumenera Corporation).

Prussian Blue staining.

Bone marrow smears were created using a Cytospin™ 4 Cytocentrifuge (Thermo Fisher Scientific Waltham, MA USA) using 100,000 cells/slide at 400xg for 5 minutes. The smears were subsequently stained for iron detection using an Iron Stain Kit (Prussian Blue Stain) (ab150674) (Abcam, Cambridge, UK), following the manufacturer's instructions. Imaging has been conducted using a Leica DM4000B upright imaging scope with a Leica DFC7000 T Camera and LAS X Life Science Microscope Sofware Platform (Leica Microsystems, Wetzlar, Germany).

Droplet Digital PCR (ddPCR) for Analysis of VCN and Alas2 deletion.

Droplet Digital PCR (ddPCR) was performed using a BioRad QX200 Droplet Digital PCR System (BioRad, Hercules, CA). The Vector Copy Number analysis was performed with a double-probe assay, using *Psi* to detect the lentiviral *Psi* packaging sequence and a portion of the *PCBP2* gene intron conserved among 17 species as the housekeeping gene.[9,10] Viral potency was calculated using the formula MOI = VCN x number of cells x Dilution Factor. The *Alas2* allelic deletion was performed with a probe/primer set specific for the region between exon 5 and exon 6 of *Alas2* (**Tab. S2**).

RNA Extraction and Quantitative Real-Time PCR Analysis

RNA extraction and quantitative real-time PCR (qRT-PCR) analyses were performed as previously described.[11] Briefly, total RNA was extracted using PureLink RNA Mini Kit (Thermo Fisher Scientific, Waltham, MA USA), and 0.5-1 ug of total RNA was transcribed into complementary DNA (cDNA) by High-Capacity cDNA Reverse Transcription Kit (Thermo Fisher Scientific, Waltham, MA USA). qRT-PCR was performed using gene-specific TaqMan™ Gene Expression Assays (Thermo Fisher Scientific Waltham, MA USA) (**Tab. S4**). qRT-PCR was performed on a 7900HT Fast Real-Time PCR System (Thermo Fisher Scientific, Waltham, MA USA), and the analyses were done using RQ Manager software. Transcript abundance, normalized to 18s messenger (Rps18) or β-actin (Actb) ribonucleic acid (mRNA) expression, is expressed as a fold increase over a calibrator sample.

Flow cytometry.

Flow cytometry was performed using a BD FACSCalibur (BD Biosciences, Franklin Lakes, NJ) instrument. Erythroid populations were characterized using FITC Anti-Mouse CD71 (113806) and APC Anti-Mouse Ter119 (116212), PE Anti-Human/Mouse CD44 (103008), as well as 7-AAD Viability Staining Solution (420404) (Biolegend, San Diego, CA). Donor chimerism was determined using PE Anti-Mouse CD45.2 (12-0454-82) (ThermoFisher, Waltham, MA) antibody for the donor and APC Anti-Mouse CD45.1 (110714) (Biolegend, San Diego, CA) antibody for the recipient. The flow cytometry results were analyzed using FlowJo™ v10.8 Software (BD Life Sciences).

Pathology assessment.

Four-micron-thick liver, spleen, and bone marrow sections were stained with hematoxylin and eosin for morphological assessment and Prussian blue stain to detect iron. The slides were scanned using the Aperio Versa 200 slide scanner, and a positive pixel count algorithm was used to quantify the level of iron accumulation in organs.

Electron microscopy

Tissues for electron microscopic examination were fixed with 2.5% glutaraldehyde and 2.0% paraformaldehyde in 0.1M sodium cacodylate buffer, pH 7.4, overnight at 4ºC. After subsequent buffer washes, the samples were post-fixed in 2.0% osmium tetroxide for 1 hour at room

temperature and rinsed in DH2O before *en bloc* staining with 2% uranyl acetate. After dehydration through a graded ethanol series, the tissue was infiltrated and embedded in EMbed-812 (Electron Microscopy Sciences, Fort Washington, PA). Thin sections were stained with uranyl acetate and lead citrate and examined with a JEOL 1010 electron microscope fitted with a Hamamatsu digital camera and AMT Advantage image capture software.

Mitochondrial cristae analysis

The evaluation of the mitochondrial cristae has been performed using the open-source platform for biological-image analysis Fiji and the Trainable Weka Segmentation plug-in.[12,13]

Enzyme-Linked Immunosorbent Assays (ELISAs) and Colorimetric Assays.

Mouse Erythroferrone (ERFE) and Hepcidin were measured in the serum using Hepcidin Murine-Compete™ ELISA Kit (ERF-200) and Hepcidin Murine-Compete™ ELISA Kit (HMC-001), respectively (Intrinsic LifeSciences, La Jolla, CA). Transferrin was evaluated in the serum using a Mouse Transferrin ELISA Kit (ab157724) (Abcam, Cambridge, UK). Erythropoietin (EPO) was measured in the serum using a Mouse Erythropoietin/EPO Quantikine ELISA Kit (MEP00B) (R&D Systems, Inc., Minneapolis, MN). Iron, UIBC, and TIBC were evaluated using Iron/TIBC Reagents (I750460) (Pointe Scientific, Canton, MI). Ferritin was assessed in the serum using a Mouse Ferritin ELISA Kit (FTL) (ab157713) (Abcam, Cambridge, UK). All the described tests were conducted according to manufacturers' instructions.

Data analysis

Data analysis was performed using GraphPad Prism 10 Version 10.1.0 for MacOS, GraphPad Software, Boston, Massachusetts USA, www.graphpad.com

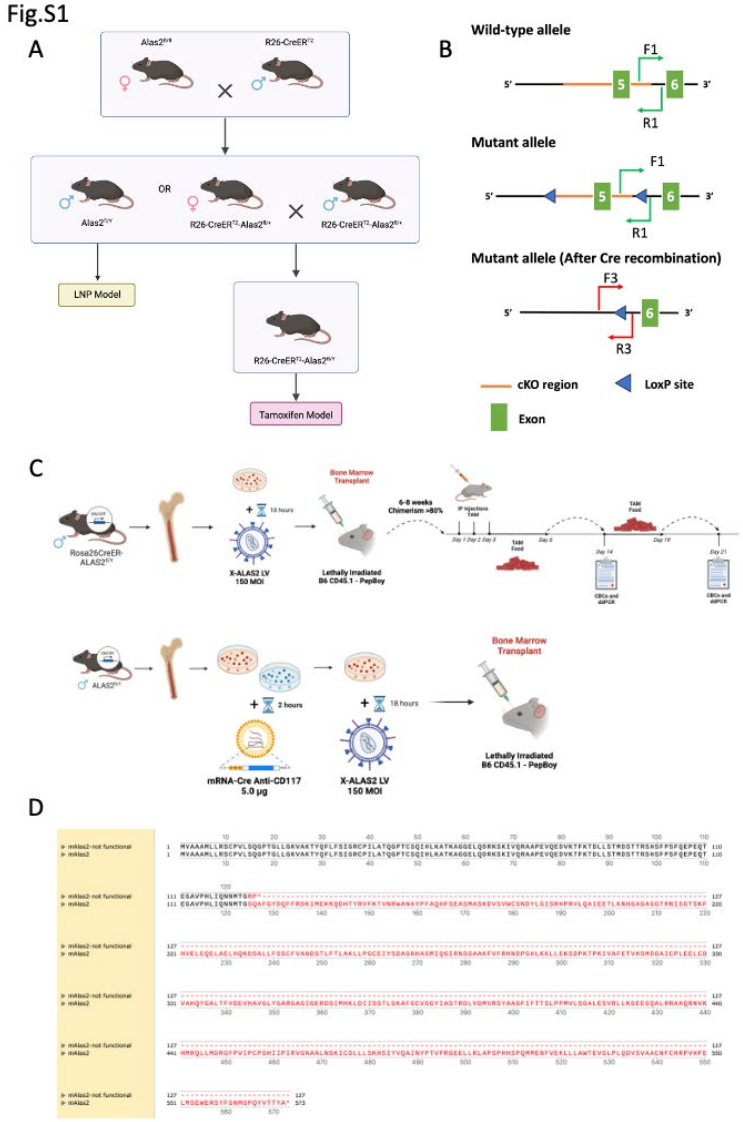

Supplementary Figures

Fig. S1 (A) Schematic representation of the breeding process to obtain R26-CreER^{T2}-*Alas2*$^{fl/Y}$ mice crossing *Alas2*$^{fl/fl}$ and B6.129-Gt(ROSA)$^{26Sortm1(cre/ERT2)}$Tyj/J (R26-CreER^{T2}) created with Biorender.com (Agreement IJ261HCIAT). The R26-CreER^{T2}-*Alas2*$^{fl/Y}$ mice were used to obtain the murine *Alas2*-KO in the tamoxifen model, while the *Alas2*$^{fl/Y}$ mice obtained from the same breeding were used to obtain the murine *Alas2*-KO in the LNP^{CD117}Cre Model. **(B)** Schematics of the *Alas2* allele in the absence or presence of the LoxP sites and after the Cre recombination, including primer localizations. *Alas2*$^{fl/fl}$ transgenic animals were generated with Taconic Biosciences (Germantown, NY, USA). **(C)** Schematic representation of generation and timeline for the tamoxifen model (A) and the LNP^{CD117}Cre model (B) created with Biorender.com (Agreement SC261HCM8G). **(D)** The aminoacidic sequence in functional (bottom) and non-functional (top) ALAS2 protein, following Cre recombinase, created with SnapGene® software (from Dotmatics; available at snapgene.com). The red sequence highlights the missing sequence in the non-functional protein due to a stop codon at AA26. The stop codon is indicated by * (top).

Fig.S2

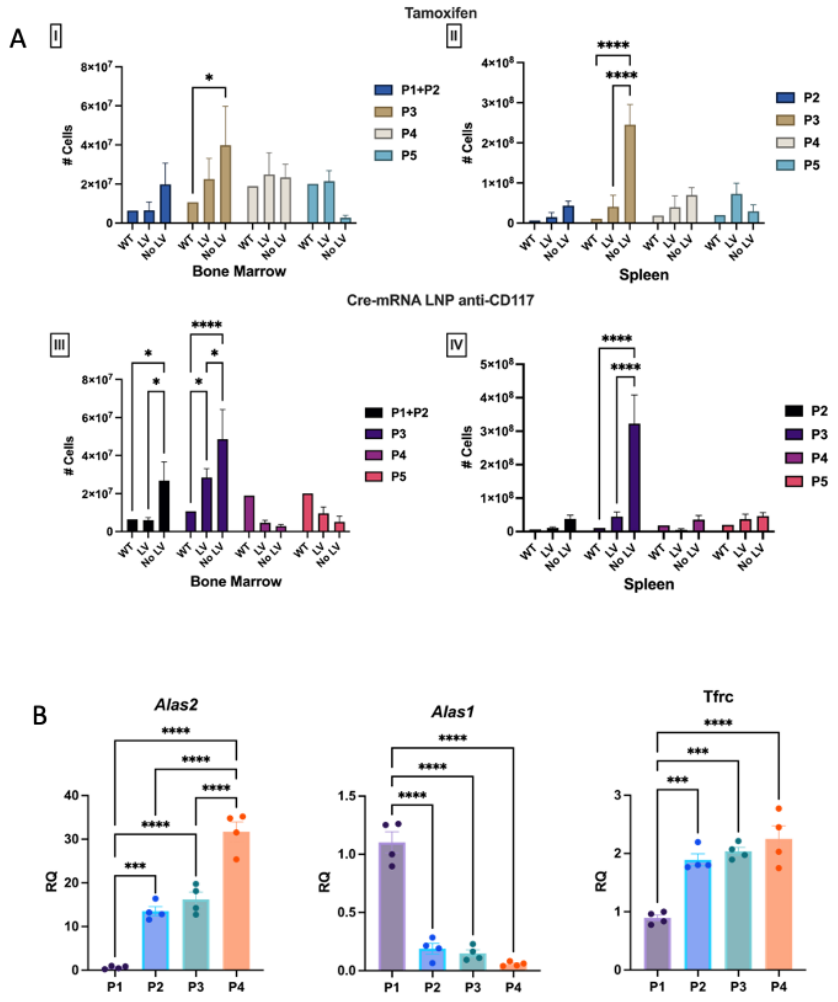

335 **Fig. S2 (A)** Absolute cell count of erythroid populations in BM and spleen of animals treated (LV)
336 or not treated (no LV) with X-ALAS2-LV (N=9 in all experimental groups), using the TAM or
337 LNP^{CD117}Cre treatment at endpoint. P1+P2/P2 = Proerythroblasts/basophilic erythroblasts; P3 =
338 Polychromatic erythroblasts; P4: Orthochromatic erythroblasts/reticulocytes; P5: Erythrocytes.
339 Data are shown as Mean ± SEM. P-values are Tukey's multiple comparison test after one-way
340 ANOVA *p<0.05, ****p<0.0001. **(B)** RQ-PCR expression analysis of *Alas2*, *Alas1*, and *Tfrc* in
341 isolated erythroid populations in the bone marrow of wild-type animals. P1 = Proerythroblasts; P2
342 = Basophilic erythroblasts; P3 = Polychromatic erythroblasts; P4 = Orthochromatic erythroblasts.
343 N = 4 C57/BL6. Data are shown as Mean ± SEM. P-values are Tukey's multiple comparison test
344 after one-way ANOVA ***p<0.001, ****p<0.0001.

Fig.S3

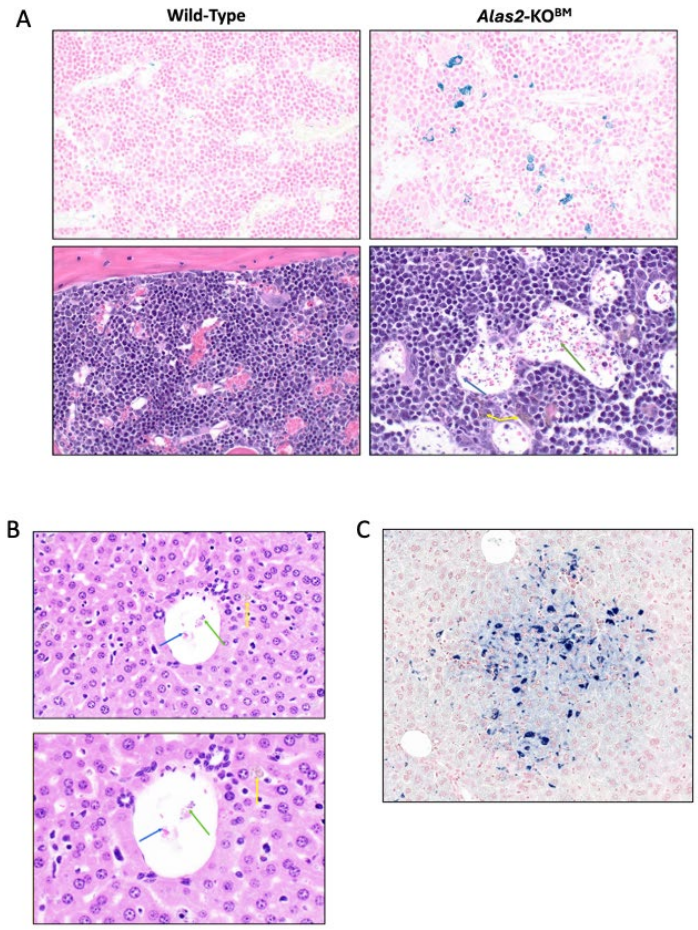

Fig. S3. **(A) Top:** Representative Prussian blue staining imagining of bone marrow tissue. *Alas2*-KO^{BM} (top right) shows the presence of hemosiderin (blue) compared to the control (top left). Magnification 40x. **Bottom:** Representative hematoxylin/eosin imaging of bone marrow tissue. *Alas2*-KO^{BM} (bottom right) shows the presence of hemosiderin, microcytosis, and polychromasia compared to the control (bottom left). Yellow arrow: hemosiderin; blue arrow: polychromatophilic erythrocytes; green arrow: small and basophilic erythrocytes. Magnification 40x. **(B)** Representative hematoxylin/eosin imaging of liver tissue shows hemosiderin (yellow arrow), microcytosis, and polychromasia. Blue arrow: polychromatophilic erythrocytes; green arrow: small and basophilic erythrocytes. Magnification: top 40x, bottom 60x. **(C)** Representative Prussian blue staining imagining of liver tissue showing variably sized clusters of cells distributed randomly throughout the hepatic parenchyma with abundant cytoplasmic iron accumulation. These cells likely consist of Kupffer cells and other macrophages. The hepatocytes surrounding the clusters of iron-containing cells often showed a lower degree of cytoplasmic iron accumulation.

Fig.S4

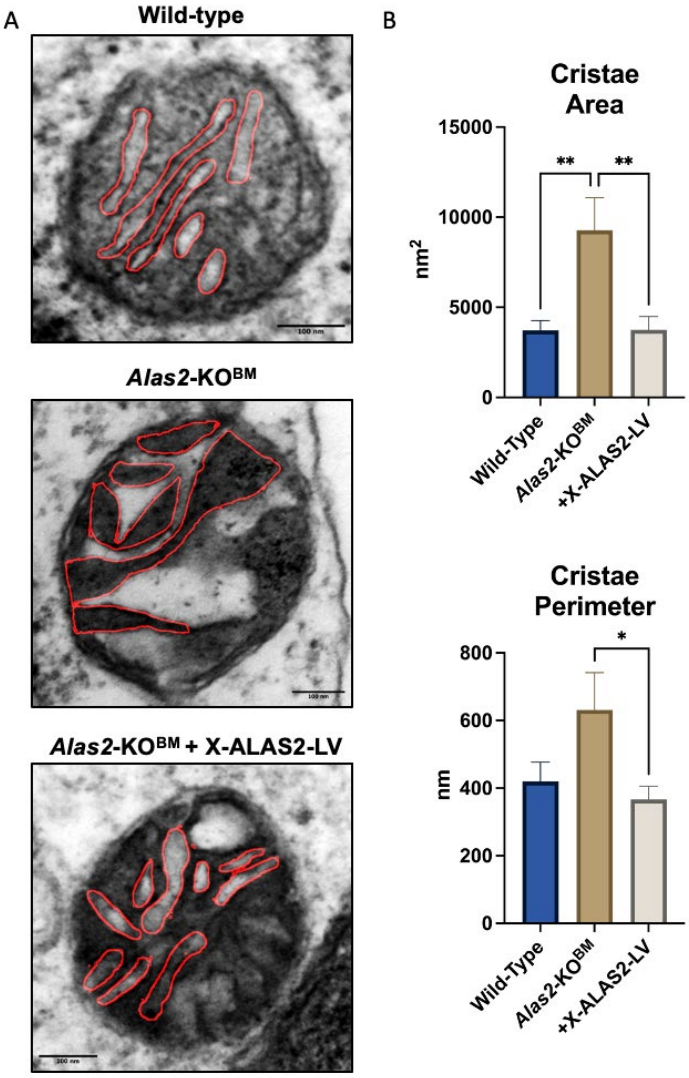

Fig. S4 (A) Representative magnified images acquired via electron microscopy of isolated P3 cells from wild-type, *Alas2*-KO^{BM}, and X-ALAS2-LV-treated animals. The red line defines the cristae's structure and shows a perturbed unfolded structure in the *ALAS2*-KO^{BM} sample compared to the WT. In X-ALAS2-LV-treated mice, the cristae structure is significantly improved. Scale bar 100 nm. **(B)** Quantification of the mitochondrial cristae area and perimeter. The *Alas2*-KO^{BM} animals show increased area and perimeter due to the perturbed unfolded structure. N = 3. Data are shown as Mean ± SEM. P-values are Tukey's multiple comparison test after one-way ANOVA *p<0.05, **p<0.01.

Fig.S5

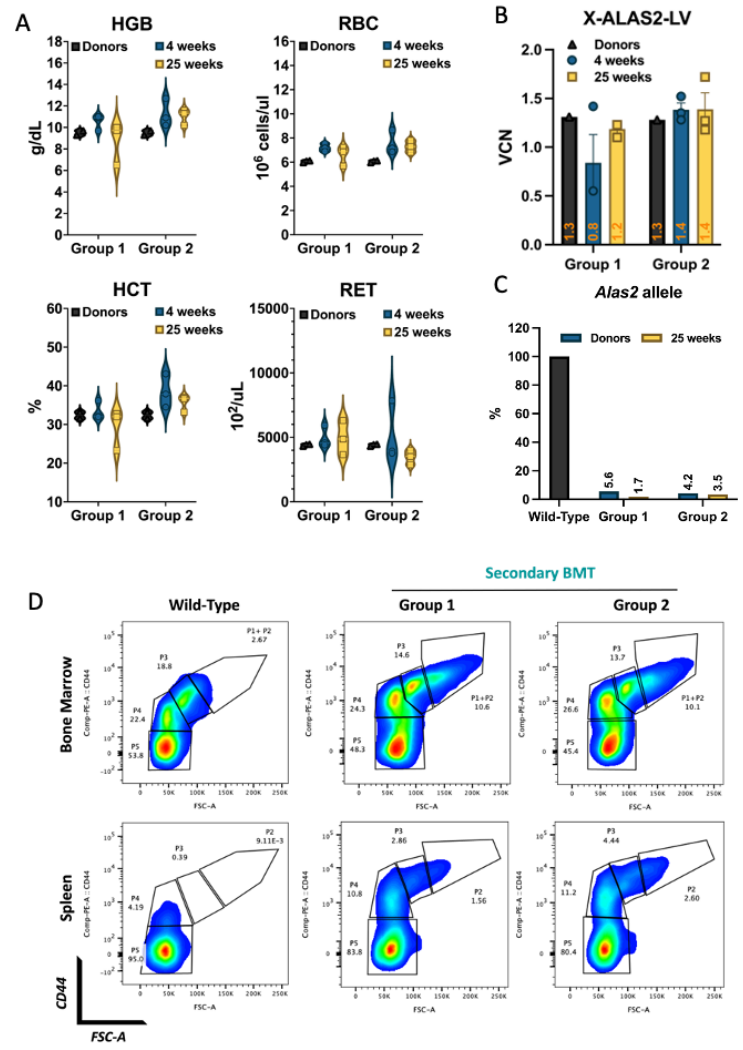

Fig. S4 (A) Hb, RBC, HTC, and reticulocytes (RET) values measured 4 and 25 weeks after BM secondary transplantation (N= 2 for donors group; N=3 in secondary transplanted mice Group 1 and Group 2). Data are shown as Mean ± SEM. P-values are Tukey's multiple comparison test after one-way ANOVA *p<0.05. **(B)** VCN quantification at 4- and 25-weeks post-transplantation in bone marrow samples from secondary chimeras (N=3 in Group 1 and Group 2). Secondary transplant mice show the original donors' VCN at 25 weeks post-transplantation. Data are shown as Mean ± SEM. **(C)** m*Alas2* allelic quantification in BM samples 25 weeks after secondary transplant (N=3 in Group 1 and Group 2). Data are shown as Mean ± SEM. P-values are Tukey's multiple comparison test after one-way ANOVA *p<0.05, ** p<0.01. **(D)** Representative flow cytometry analysis of BM and spleen erythroid populations (defined as FSC-A/CD-44 within the Ter119 subcompartment) in secondary BM transplants. Data are shown as. P1+P2/P2 = Pro erythroblasts/basophilic erythroblasts; P3 = Polychromatic erythroblasts; P4: Orthochromatic erythroblasts/reticulocytes; P5: Erythrocytes.

382 **Supplementary Tables**

383

384 **Tab. S1 Primer sequences for *Alas2* and R26CreER^{T2}**

Primers for genotyping		
Alas2	**Conditional KO**	**Constitutive KO**
Forward	AACTAAGTCAGCCAACATATCATGC	AAGAGACACAGCTAGAAACTAGGTC
Reverse	GTAGAGGAAAGAAGGAGACACGTAG	ATGAAAGCCTTCCTTAATGTGGTCA
R26CreER^{T2}		
Wild-type Forward	AAAGTCGCTCTGAGTTGTTAT	
Mutant Forward	GGAGCGGGAGAAATGGATATG	
Common Reverse	CCTGATCCTGGCAATTTCCG	

ALAS2	TCAGGCATAGGTGGTGACATACTGGGGCCCCATGTTCCCGAAGTAGGAACGTTC CCACTCACTCATGAGCTCAAAGTGTACAGGACGGCGACAGAAATTGCAGGCAG CCACAGACACATCCTGGAGGGGCAGCCCCACCGCAGTCCAAGCCAGCAGCAGC TTCTCCACAAAATCTTCCATCATCTGAGGGCTGTGGTGGGGGGAGGGTGCCAAG CGCAGGAGCTCTTCACCCCGGGGGACAGTTGGGTAGTTGATGGCCTGCACATAG ATGCCATGCTTGGAGAGCAGGAGATCACAGAGCTTGCTGTTGAGTGCTGCATTG CCCACCCGGATGGGGATGATGTGGCTGGGGCAGGGGATGACAGGAAGGCCCCT GTCCATGAGTAGCTGGCGCATGTGCTTGACATTGCGCTGGTGGGCTCGCCTCAG GGCTTGGCCCTCCTCTCCCTTGAGCAGCCGCACAGATTCTAGAGCTCCAGAGAG CACCATGGGGGGCAGAGAAGTGGTAAAGATGAAGCCTGCAGCATAGGAGCGCA CCATGTCCACCAAGTCACGGGTGCTGGCAATGTAGCCGCCCACACAGCCAAAGG CCTTGCCAAGAGTTCCAGAGATGATGTCAATCTTATGCATAATTCCATCACGCTC CCCAATCCCAGCGCCCCGGGACCCATACAGTCCTACAGCATGGACCTCATCCAC GAAGGTCAGGGCCCCATACTGGTGGGACACATCACACAACTCCTCGAGGGGAC AGATGGCACCATCCATGGAGTGGACAGTCTCAAAGGCCACAATTTTGGGTATCT TAGGGTTAGACTTCTCTAGAAGTTTCTTTAGGTGGTCAGGGTCATTGTGCCTGAA GACAAACTTGGCTGCTCCACTGTTACGGATACCTTGGATCATGGAAGCATGGTT GCCTGCGTCTGAGTAAATCTCGCACCCTGGCAGGATCTTGGCCAAGGTGAAGAG AGTAGAGTCATTGGCAACAAAGCAGGAGGAGAAGAGCAGGGCTGAGTCCTTCT GGTGCAGCTCAGCCAGCTCCTGCTCAAGCTCCACATGAAACTTACTGGTGCCTG AGATGTTGCGGGTGCCACCAGCTCCAGCACCATGACGCTGCAGGGTCTCCTGTG TGGCTTGCAAGACCTGAGGGTGTCGGCTCATGCCCAGGTAATCATTACTACACC AGACGGACACATCCTTTGAGGCCACAGATGCCTCAGAGAAATGTTGGGCAAAG GGATATGCATCAGCCCAGCGGTTCACAGTCTTGAACACACGGTAGGTGTGATCC TGTTTCTTCTCCATGATCTTGTCCCTGAAAAACTGGTCATAACTGAAGACATAGT TTCCAGGCATATTGTTCTGAATCAGGTGTGTGACCTTCCCAGAGATCTGCTCCTG CTCCTGGGGACCGGAAAATGGCTTCCTTAGGCTGACTGAGACCAGGGAGCTAGG CAGATCTGTCTTGAAAGCCTTCACATCTTCCTGGACTTCTGGGGCTGCCTTCTGC ACAATCTTGCTCTTCCCATCCTGGAGTTCCGACAGCATGAAGGGACAGTGGCCC TTCGCCCAAGATGGAGAATCTCCTCCAGCCTTTGTTGCCTTAAGGTGGATTTGAG AACAGTTTGGTCCTTGGGTAGCCAGGATGGGACAGCGTCCAATACCAAACAGG AACTGGTGAGTCTTAACCACCTTGCCTAGGAGGCTTGTGGGGCCCCGGGCAAGC ACTGGGCAGCACTGTAGCAGCATGGCTGCAGTCACCAT

HBB3 Enhancer	TAGGTATTGAATAAGAAAAATGAAGTTAAGGTGGTTGATGGTAACACTATGCTA ATAACTGCAGAGCCAGAAGCACCATAAGGGACATGATAAGGGAGCCAGCAGAC CTCTGATCTCTTCCTGAATGCTAATCTTAAACATCCTGAGGAAGAATGGGACTTC CATTTGGGGTGGGCCTATGATAGGGTAATAAGACAGTAGTGAATATCAAGCTAC AAAAAGCCCCCTTTCAAATTCTTCTCAGTCCTAACTTTTCATACTAAGCCCAGTC CTTCCAAAGCAGACTGTGAAAGAGTGATAGTTCCGGGAGACTAGCACTGCAGAT TCCGGGTCACTGTGAGTGGGGGAGGCAGGGAAGAAGGGCTCACAGGACAGTCA AACCATGCCCCCTGTTTTTCCTTCTTCAAGTAGACCTCTATAAGACAACAGAGAC AACTAAGGCTGAGTGGCCAGGCGAGGAGAAACCATCTCGCCGTAAAACATGGA AGGAACACTTCAGGGGAAAGGTGGTATCTCTAAGCAAGAGAACTGAGTGGAGT CAAGGCTGAGAGATGCAGGATAAGCAAATGGGTAGTGAAAAGACATTCATGAG GACAGCTAAAACAATAAGTAATGTAAAATACAGCATAGCAAAACTTTAACCTCC AAATCAAGCCTCTACTTGAATCCTTTTCTGAGGGATGAATAAGGCATAGGCATC AGGGGCTGTTGCCAATGTGCATTAGCTGTTTGCAGCCTCACCTTCTTTCATGGAG TTTAAGATATAGTGTATTTTCCCAAGGTTTGAACTAGCTCTTCATTTCTTTATGTT TTAAATGCACTGACCTCCCACATTCCCTTTTTAGTAAAATATTCAGAAATAATTT AAATACATCA
HBB Promoter	TAGATTGGCCAACCCTAGGGTGTGGCTCCACAGGGTGAGGTCTAAGTGATGACA GCCGTACCTGTCCTTGGCTCTTCTGGCACTGGCTTAGGAGTTGGACTTCAAACCC TCAGCCCTCCCTCTAAGATATATCTCTTGGCCCCATACCATCAGTACAAATTGCT ACTAAAAACATCCTCCTTTGCAAGTGTATTTAC

HS2	CCTTTTGCCACCTAGCTGTCCAGGGGTGCCTTAAAATGGCAAACAAGGTTTGTTT TCTTTTCCTGTTTTCATGCCTTCCTCTTCCATATCCTTGTTTCATATTAATACATGT GTATAGATCCTAAAAATCTATACACATGTATTAATAAAGCCTGATTCTGCCGCTT CTAGGTATAGAGGCCACCTGCAAGATAAATATTTGATTCACAATAACTAATCAT TCTATGGCAATTGATAACAACAAATATATATATATATATATATACGTATATGTGT ATATATATATATATATATTCAGGAAATAATATATTCTAGAATATGTCACATTCTG TCTCAGGCATCCATTTTCTTTATGATGCCGTTTGAGGTGGAGTTTTAGTCAGGTG GTCAGCTTCTCCTTTTTTTTGCCATCTGCCCTGTAAGCATCCTGCTGGGGACCCA GATAGGAGTCATCACTCTAGGCTGAGAACATCTGGGCACACACCCTAAGCCTCA GCATGACTCATCATGACTCAGCATTGCTGTGCTTGAGCCAGAAGGTTTGCTTAG AAGGTTACACAGAACCAGAAGGCGGGGGTGGGGCACTGACCCCGACAGGGGCC TGGCCAGAACTGCTCATGCTTGGACTATGGGAGGTCACTAATGGAGACACACAG AAATGTAACAGGAACTAAGGAAAAACTGAAGCTTATTTAATCAGAGATGAGGA TGCTGGAAGGGATAGAGGGAGCTGAGCTTGTAAAAAGTATAGTAATCATTCAG CAAATGGTTTTGAAGCACCTGCTGGATGCTAAACACTATTTTCAGTGCTTGAATC ATAAATAAGAATAAAACATGTATCTTATTCCCCACAAGAGTCCAAGTAAAAAAT AACAGTTAATTATAATGTGCTCTGTCCCCCAGGCTGGAGTGCAGTGGCACGATC TCAGCTCACTGCAACCTCCGCCTCCCGGGTTCAAGCAATTCTCCTGCCTCAGCCA CCCTAATAGCTGGGATTACAGGTGCACACCACCATGCCAGGCTAATTTTTGTAC TTTTTGTAGAGGTTTTGTACTTTTTGTAGAGGCAGGGTATCACCATGTTGTCCAA GATGGTCTTGAACTCCTGAGCTCCAAGCAGTCCACCCACCTCAGCCTCCCAAAG TGCTGGGATTACAGGTGTGAGACACCATGCCCAGATTTTCCATATTTAATAGAG GTATTTATGGGATGGGGGAAAAGAATGTTTCTCTCACTGTGGATTATTTTAGAG AGTGGAGAATGGTCAAGATTTTTTTAAAAATTAAGAAAACATAAGTTGGACCTT GAGAAATGAAAATTTATTTTTTTGTTGGAGGATACCCATTCTCTATCTCCCATCA GGGCAAGCTGTAAGGAACTGGCTAAGACACAGTGAGACAGAGTGACTTAGTCT TAGAGGCCCCACTGGTACGACG

HS3	AAGCTTTCATTAAAAAAAGTCTAACCAGCTGCATTCGACTTTGACTGCAGCAGC TGGTTAGAAGGTTCTACTGGAGGAGGGTCCCAGCCCATTGCTAAATTAACATCA GGCTCTGAGACTGGCAGTATATCTCTAACAGTGGTTGATGCTATCTTCTGGAACT TGCCTGCTACATTGAGACCACTGACCCATACATAGGAAGCCCATAGCTCTGTCC TGAACTGTTAGGCCACTGGTCCAGAGAGTGTGCATCTCCTTTGATCCTCATAATA ACCCTATGAGATAGACACAATTATTACTCTTACTTTATAGATGATGATCCTGAAA ACATAGGAGTCAAGGCACTTGCCCCTAGCTGGGGGTATAGGGGAGCAGTCCCAT GTAGTAGTAGAATGAAAAATGCTGCTATGCTGTGCCTCCCCCACCTTTCCCATGT CTGCCCTCTACTCATGGTCTATCTCTCCTGGCTCCTGGGAGTCATGGACTCCACC CAGCACCACCAACCTGACCTAACCACCTATCTGAGCCTGCCAGCCTATAACCCA TCTGGGCCCTGATAGCTGGTGGCCAGCCCTGACCCCACCCCACCCTCCCTGGAA CCTCTGATAGACACATCTGGCACACCAGCTCGCAAAGTCACCGTGAGGGTCTTG TGTTTGCTGAGTCAAAATTCCTTGAAATCCAAGTCCTTAGAGACTCCTGCTCCCA AATTTACAGTCATAGACTTCTTCATGGCTGTCTCCTTTATCCACAGAATGATTCC TTTGCTTCATTGCCCCATCCATCTGATCCTCCTCATCAGTGCAGCACAGGGCCCA TGAGCAGTAGCTGCAGAGTCTCACATAGGTCTGGCACTGCCTCTGACATGTCCG ACCTTAGGCAAATGCTTGACTCTTCTGAGCTCAGTCTTGTCATGGCAAAATAAA GATAATAATAGTGTTTTTTTATGGAGTTAGCGTGAGGATGGAAAACAATAGCAA AATTGATTAGACTATAAAAGGTCTCAACAAATAGTAGTAGATTTTATCATCCAT TAATCCTTCCCTCTCCTCTCTTACTCATCCCATCACGTATGCCTCTTAATTTTCCC TTACCTATAATAAGAGTTATTCCTCTTATTATATTCTTCTTATAGTGATTCTGGAT ATTAAAGTGGGAATGAGGGGCAGGCCACTAACGAAGAAGATGTTTCTCAAAGA AGC
Ankyrin Insulator	GTGCGGGCCAGGCCCCCGAGGGCCTTATCGGCCCCAGAGGCGCTTGCTGTCGGG CCGGGCGCTCCCGGCACGGGCGGGCGGAGGGGTGGCGCCCGCCTGGGGACCGC AGATTACAAGAGCACCTCCTCCCCCAACCCCAGGAGGCCCCGCTCCCCAGGCCT CGGCCGGCGCGGACCCCTGGTTGCCCCGG

385 **Tab. S2 Sequences on the main features contained in X-ALAS2 lentiviral vector**

ddPCR probes		
	Psi	***Alas2*-KO**
Forward	ACTTGAAAGCGAAAGGGAAAC	CCCTTTGCCCAACACTTCTC
Reverse	CGCACCCATCTCTCTCCTTCT	ACAAAAGAAGTGGCAGCAGAA
Probe	AGCTCTCTCGACGCAGGACTCGGC	AGGCCATAGAGTAAGTAGTAGAGTGTGGAC
Fluorophore	FAM	FAM
	PCBP2*	
Forward	CCAGTCTGCTTGGCATGAAA	
Reverse	GGTACCCTTAGCAGCAGACA	
Probe	CCCATCCCTCTCCTGGCTCTAA	
Fluorophore	HEX	

386 **Tab. S3 Probes and primer sets used for vector copy number analysis (PSI) and *Alas2* allelic**
387 **deletion analysis (KO). *PCBP2 has been used as a housekeeping probe/primer set**

Gene	Assay ID	Fluorofore
Bax	Mm00432051_m1	FAM-MGB
Bak	Mm00432045_m1	FAM-MGB
Bid	Mm00432073_m1	FAM-MGB
Casp9	Mm00516563_m1	FAM-MGB
Casp3	Mm01195085_m1	FAM-MGB
Casp7	Mm00432322_m1	FAM-MGB
Bcl-2	Mm00477631_m1	FAM-MGB
Bbc3	Mm00519268_m1	FAM-MGB
Tnf	Mm00443258_m1	FAM-MGB
L-6	Mm00446190_m1	FAM-MGB
Hmox1	Mm00516005_m1	FAM-MGB
Hkdc1	Mm00520597_m1	FAM-MGB
Pfkp	Mm00444792_m1	FAM-MGB
Pkm	Mm00834102_gH	FAM-MGB
Ldha	Mm01612132_g1	FAM-MGB
Uqcrfs1	Mm00481849_m1	FAM-MGB
Cycs	Mm01621048_s1	FAM-MGB
ALAS2	Hs01085701_m1	FAM-MGB
Alas2	Mm00802083_m1	FAM-MGB
Alas1	Mm01235914_m1	FAM-MGB
Trfc	Mm00441941_m1	FAM-MGB
Rps18	Mm02601777_g1	FAM-MGB
Actb	Mm02619580_g1	FAM-MGB

388 **Tab. S4 TaqMan Probes used for qRT-PCR analysis.**

References

1. Xu X, Tassone B, Ostano P, et al. HSD17B7 gene in self-renewal and oncogenicity of keratinocytes from Black versus White populations. *EMBO Mol Med*. 2021;13(7):e14133.
2. Bergonia HA, Franklin MR, Kushner JP, Phillips JD. A method for determining delta-aminolevulinic acid synthase activity in homogenized cells and tissues. *Clin Biochem*. 2015;48(12):788-795.
3. Sharma B. Kinetic Characterisation of Phosphofructokinase Purified from Setaria cervi: A Bovine Filarial Parasite. *Enzyme Res*. 2011;2011:939472.
4. Riganti C, Aldieri E, Bergandi L, et al. Crocidolite asbestos inhibits pentose phosphate oxidative pathway and glucose 6-phosphate dehydrogenase activity in human lung epithelial cells. *Free Radic Biol Med*. 2002;32(9):938-949.
5. Capello M, Ferri-Borgogno S, Riganti C, et al. Targeting the Warburg effect in cancer cells through ENO1 knockdown rescues oxidative phosphorylation and induces growth arrest. *Oncotarget*. 2016;7(5):5598-5612.
6. Vlatkovic I, Ludwig J, Boros G, et al. Ribozyme Assays to Quantify the Capping Efficiency of In Vitro-Transcribed mRNA. *Pharmaceutics*. 2022;14(2).
7. Maier MA, Jayaraman M, Matsuda S, et al. Biodegradable lipids enabling rapidly eliminated lipid nanoparticles for systemic delivery of RNAi therapeutics. *Mol Ther*. 2013;21(8):1570-1578.
8. Breda L, Papp TE, Triebwasser MP, et al. In vivo hematopoietic stem cell modification by mRNA delivery. *Science*. 2023;381(6656):436-443.
9. Makeyev AV, Chkheidze AN, Liebhaber SA. A set of highly conserved RNA-binding proteins, alphaCP-1 and alphaCP-2, implicated in mRNA stabilization, are coexpressed from an intronless gene and its intron-containing paralog. *J Biol Chem*. 1999;274(35):24849-24857.
10. Christodoulou I, Patsali P, Stephanou C, Antoniou M, Kleanthous M, Lederer CW. Measurement of lentiviral vector titre and copy number by cross-species duplex quantitative PCR. *Gene Ther*. 2016;23(1):113-118.
11. Petrillo S, De Giorgio F, Bertino F, et al. Endothelial cells require functional FLVCR1a during developmental and adult angiogenesis. *Angiogenesis*. 2023;26(3):365-384.
12. Schindelin J, Arganda-Carreras I, Frise E, et al. Fiji: an open-source platform for biological-image analysis. *Nat Methods*. 2012;9(7):676-682.
13. Arganda-Carreras I, Kaynig V, Rueden C, et al. Trainable Weka Segmentation: a machine learning tool for microscopy pixel classification. *Bioinformatics*. 2017;33(15):2424-2426.